

1 **Modeling and sensitivity analysis of transport and**
2 **deposition of radionuclides from the Fukushima Daiichi**
3 **accident**

4
5 **Xiaofeng Hu ^{1,2}, Dan Li ³, Hong Huang ¹, Shifei Shen¹ and Elie Bou-Zeid ²**

6 [1] Institute of Public Safety Research, Department of Engineering Physics, Tsinghua
7 University, Beijing, China

8 [2] Department of Civil and Environmental Engineering, Princeton University, Princeton,
9 New Jersey, USA

10 [3] Program of Atmospheric and Oceanic Sciences, Princeton University, Princeton, New
11 Jersey, USA

12 Correspondence to: Hong Huang (hhong@mail.tsinghua.edu.cn)

13

14 **Abstract**

15 The atmospheric transport and ground deposition of radioactive isotopes ¹³¹I and ¹³⁷Cs during
16 and after the Fukushima Daiichi Nuclear Power Plant (FDNPP) accident (March 2011) are
17 investigated using the Weather Research and Forecasting/Chemistry (WRF/Chem) model. The
18 aim is to assess the skill of WRF in simulating these processes and the sensitivity of the
19 model's performance to various parameterizations of unresolved physics. The WRF/Chem
20 model is first upgraded by implementing a radioactive decay term into the advection-diffusion
21 solver and adding three parameterizations for dry deposition and two parameterizations for
22 wet deposition. Different microphysics and horizontal turbulent diffusion schemes are then
23 tested for their ability to reproduce observed meteorological conditions. Subsequently, the
24 influence on the simulated transport and deposition of the characteristics of the emission

25 source, including the emission rate, the gas partitioning of ^{131}I and the size distribution of
26 ^{137}Cs , is examined. The results show that the model can predict the wind fields and rainfall
27 realistically and that the ground deposition of the radionuclides can also be captured
28 reasonably well. The modeled precipitation is largely influenced by the microphysics schemes,
29 while the influence of the horizontal diffusion schemes on the wind fields is subtle. However,
30 the ground deposition of radionuclides is sensitive to both horizontal diffusion schemes and
31 microphysical schemes. Wet deposition dominated over dry deposition at most of the
32 observation stations, but not at all locations in the simulated domain. To assess the sensitivity
33 of the total daily deposition to all of the model physics and inputs, the averaged absolute
34 value of the difference (AAD) is proposed. Based on AAD, the total deposition is mainly
35 influenced by the emission rate for both ^{131}I and ^{137}Cs ; while it is not sensitive to the dry
36 deposition parameterizations since the dry deposition is just a minor fraction of the total
37 deposition. Moreover, for ^{131}I , the deposition is moderately sensitive (variations between 10%
38 and 40% between different runs) to the microphysics schemes, the horizontal diffusion
39 schemes, gas partitioning and wet deposition parameterizations. For ^{137}Cs , the deposition is
40 very sensitive (variation exceeding 40% between different runs) to the microphysics schemes
41 and wet deposition parameterizations, but moderately sensitive to the horizontal diffusion
42 schemes and the size distribution.

43

44 **1 Introduction**

45 Large amounts of radionuclides were released into the atmosphere after the nuclear accident
46 at the Fukushima Daiichi nuclear power plant (FDNPP) on March 11, 2011. Later, the
47 Japanese government reported that the radioactive materials were detected in the food and
48 water supply in Fukushima and adjacent areas (Zakaib, 2011). Radionuclides can significantly
49 jeopardize human health, causing cancer and acute radiation diseases (Till and Grogan, 2008).
50 Understanding the spatial and temporal distributions of radionuclides is key to assessing and
51 mitigating the health impact of radioactive releases; it is thus important to be able to

52 accurately model their atmospheric transport and ground deposition.

53 Over the past few decades, many numerical models have been developed and applied for
54 studying the transport and deposition of radionuclides (Andronopoulos and Bartzis, 2010;de
55 Sampaio et al., 2008;Lauritzen et al., 2007;Lutman et al., 2004;Terada and Chino,
56 2008;Leelosy et al., 2011). For this particular accident at Fukushima, the Community
57 Multi-scale Air Quality (CMAQ) model (Morino et al., 2011), the Lagrangian transport model
58 HYSPLIT and FLEXPART with meteorological conditions provided by the Weather Research
59 and Forecasting (WRF) model (Srinivas et al., 2012), and the WRF/Chem tracer model which
60 directly couples the simulation of the chemistry and meteorology (Huh et al., 2012;Huh et al.,
61 2013) have been used. These studies, together with many previous studies for other events,
62 have identified a number of meteorological variables that can significantly influence the
63 atmospheric transport and ground deposition of radionuclides, including wind and rainfall
64 (Basit et al., 2008;Mathieu et al., 2012;Takemura et al., 2011;Ten Hoeve and Jacobson,
65 2012;Yamauchi, 2012). For example, the study of Morino et al. (2011) has shown that during
66 the period from March 11 to 30, 2011, the amounts of ^{131}I and ^{137}Cs transported across the
67 eastern boundary (downwind) of their domain are 6.52×10^{16} Bq and 4.58×10^{15} Bq,
68 respectively; while those across the western boundary (upwind) are only 1.49×10^{12} Bq and
69 1.13×10^7 Bq, respectively. This illustrates how wind direction significantly affects the
70 atmospheric transport of radionuclides. Rainfall is another important factor that can influence
71 the ground deposition of radionuclides considerably. Studies of the Fukushima accident report
72 that the estimated deposition mainly occurred when frontal rain bands passed over Japan on
73 March 21 (Yasunari et al., 2011). Deposition of the radionuclides mainly occurred between 15
74 – 17 and 19 – 21 March, when heavy rainfall was observed, as reported by Srinivas et al.
75 (2012). During these days, wet deposition was significantly higher than dry deposition. Even
76 over longer periods, wet deposition usually still dominates over dry deposition. Given the
77 findings above, it is clear that an accurate simulation of meteorological fields is a necessary
78 condition for the accurate simulation of the transport and deposition of the radionuclides.

79 As illustrated by (Talbot et al., 2012), wind is usually one of the most challenging parameters
80 to simulate successfully. Furthermore, it is also quite difficult to reproduce the spatial and
81 temporal precipitation patterns in numerical models (Li et al., 2013). However, the previous
82 studies are focused on the behavior of radionuclides with the meteorological conditions
83 simply taken from some numerical weather prediction models or analysis/reanalysis products,
84 without an assessment of whether errors in the radionuclides fate and transport are linked to
85 errors in the meteorological fields or in the transport and decay models.

86 Emission rate is another critical factor that controls the rate of atmospheric transport and
87 ground deposition of radionuclides (Korsakissok et al., 2013; Morino et al., 2011; Morino et al.,
88 2013). For instance, the study of Korsakissok et al. (2013) reported that the total deposition
89 from the Fukushima accident (sum of dry and wet deposition; in this paper, it is used
90 interchangeably with ground deposition) of ^{137}Cs is less than 1.5×10^{15} Bq with the emission
91 rate estimated by (Chino et al., 2011) but more than 5.5×10^{15} Bq with the emission rate
92 estimated by (Stohl et al., 2012). The importance of using accurate estimation of emission
93 source strength has been also demonstrated by the sensitivity analyses of Morino et al. (2013).
94 However, previous studies solely focused on the emission rate, and other emission
95 characteristics such as the gas partitioning of ^{131}I were also not considered. The gaseous
96 fraction of ^{131}I was simply set as a constant such as 80% (Morino et al., 2011) and 2/3
97 (Korsakissok et al., 2013). A review (Sportisse, 2007) shows that the gaseous fraction varies
98 among different studies: 65% to 80% (Chamberlain, 1991), 50% - 65% (Clark and Smith,
99 1988), and 70% - 90% in (Baklanov and Sorensen, 2001). This review also points out that the
100 partitioning between gaseous and particulate phases is crucial for capturing the ground
101 deposition of radionuclides. Apart from the gas partitioning, the size distribution of particles
102 is another important characteristic that has not been thoroughly studied, since some deposition
103 schemes explicitly take the size distribution into account (Brandt et al., 2002).

104 In this study, to address some of the research gaps detailed above, we choose to adopt the
105 WRF/Chem framework (Grell et al., 2005), which provides multiple parameterizations for

106 different unresolved physical processes. WRF/Chem directly couples the forecasting of the
107 chemistry and meteorology, allowing the transport simulations to exploit the full spatial and
108 temporal resolutions of the meteorological simulations. This is expected to yield better results
109 than offline approaches where pre-computed meteorological fields have to be interpolated to
110 drive the chemical transport module. Meteorological fields are however not the only source of
111 uncertainty that can reduce the accuracy of transport and deposition simulations. Previous
112 studies have also shown that different dry and wet deposition parameterizations can cause
113 different deposition rates and accumulated amounts of radionuclides (see e.g. (Brandt et al.,
114 2002)). In this study, several dry and wet deposition parameterizations are thus also added to
115 the WRF/Chem model to test and intercompare their performances. Moreover, we consider
116 the emission of ^{131}I with different gaseous fractions and that of ^{137}Cs with different particle
117 size distributions. **The specific questions this study aims to answer are:**

118 (1) What model setup parameters have the largest influence on the simulated meteorological
119 fields and what is the influence of these fields on deposition?

120 (2) What is the relative importance of wet versus dry deposition, and how sensitive are they to
121 the different parameterizations?

122 (3) How sensitive are the modeled deposition to the imposed emission rates and
123 characteristics, including the gas partitioning of ^{131}I and the size distribution of ^{137}Cs ?

124 (4) How close can model results get to observed deposition given the uncertainties in model
125 physics and inputs, and which of these uncertainties is the most critical?

126 This paper is organized in the following way: Section 2 describes the improvement to the
127 WRF/Chem model and the configuration of the simulations. In Section 3, the results are
128 presented and discussed. Section 4 presents a summary and conclusions.

129

130 2 Methodology and datasets

131 2.1 Emissions

132 Two emission datasets are used in the simulations: (1) the estimate from the Japan Atomic
133 Energy Agency (JAEA) and (2) the estimate from the Tokyo Electric Power Company
134 (TEPCO). JAEA (Katata et al., 2012;Terada et al., 2012) estimated the release period,
135 duration and emission rate of ^{131}I and ^{137}Cs from a combination of observational data and
136 atmospheric simulations using the System for Prediction of Environmental Emergency Dose
137 Information (SPEEDI). TEPCO (2012) estimated the amount of ^{131}I and ^{137}Cs released to the
138 atmosphere using their company's atmospheric dispersion calculation program Dose
139 Information Analysis for Nuclear Accident (DIANA) and the air dose rate measured from a
140 monitoring car that moved around the FDNPP. The emission rates of ^{131}I and ^{137}Cs from 0
141 UTC on March 11 to 23 UTC on March 31 from the two datasets are shown in Fig.1. The
142 emission rate for TEPCO used in this paper is calculated based on the release amount and
143 duration provided by TEPCO. Since the time interval of the emission input for the
144 WRF/Chem model is 1 hour, the emission rate over 1 hour intervals is then computed for
145 TEPCO from the data plotted in Fig.1. If a period for a specific emission rate is less than 1
146 hour, it is treated as 1 hour and the emission rate is computed as the emission amount (during
147 this period) divided by 1 hour.

148 As can be seen from Fig.1, the emission rate estimated by JAEA is continuous over the
149 simulation period while the emission rate estimated by TEPCO is discontinuous. The most
150 significant release estimated by JAEA covers the period from March 12 to March 15 with the
151 peak value on March 15, while from TEPCO's estimation the peak occurs on March 16. In
152 our simulations, the source is assumed to be a point source at 37.5 N, 141.0 E. Moreover, all
153 ^{137}Cs is assumed to be in particulate phase with different size distributions, while the gaseous
154 fraction of ^{131}I varies in different simulations. Note that particle size distributions and the gas
155 partitioning may change during the transport and deposition processes; however, this is not
156 considered in our simulations due to a lack of measurements or studies to allow us to

157 represent this change.

158

159 2.2 Simulation model

160 In WRF/Chem, advection, turbulent diffusion, emission, radioactive decay and wet deposition
161 are described using the following Eulerian advection-diffusion-reaction equation:

$$162 \quad \frac{\partial A}{\partial t} + \nabla \cdot (\mathbf{u}A) = \nabla \cdot \left(\rho \mathbf{K} \nabla \left(\frac{A}{\rho} \right) \right) - \Lambda^s A - \lambda A + E \quad (1)$$

163 where A is the air concentration (Bq m^{-3}), which represents the radioactivity per unit volume
164 equivalent to the number of radionuclides that decay per second in a unit volume. Λ^s is the
165 wet scavenging rate (s^{-1}); λ represents the (first-order) radioactive decay rate (s^{-1}) and E is the
166 point source for the radionuclides. \mathbf{K} is the turbulent diffusivity tensor, which includes the
167 effect of dry deposition. Note that WRF treats the flow as fully compressible. The total
168 number of the radionuclides per m^3 at $t = 0$ can be calculated from the following equation

$$169 \quad N_0 = \frac{A_0}{I} \quad (2)$$

170 In WRF/Chem, the unit used for transport of gases is ppmv and the unit for transport of
171 aerosols is $\mu\text{g kg}^{-1}$. However, the unit used in the emission module is Bq m^{-3} , which is
172 consistent with the unit used in the emission files from JAEA and TEPCO. Therefore, in order
173 to use the default units to calculate the atmospheric transport of the radionuclides, a unit
174 conversion is necessary for input of emissions to WRF, and then to convert its output into
175 Bq m^{-3} . Based on the Eq. (2):

$$176 \quad \frac{W_I}{V_m} = \frac{A_I}{I_I \text{NA}} 10^6 \quad (3)$$

$$177 \quad \frac{W_{\text{Cs}}}{M_{\text{Cs}}} = \frac{A_{\text{Cs}}}{I_{\text{Cs}} \text{NA} r_{\text{air}}} 10^6 \quad (4)$$

178 where W_I is the air concentration of ^{131}I in ppmv; W_{Cs} is the air concentration of ^{137}Cs in
 179 $\mu\text{g kg}^{-1}$; A_I (Bq m^{-3}) is the air concentration of ^{131}I in Bq m^{-3} ; A_{Cs} is the air concentration of
 180 ^{137}Cs in Bq m^{-3} ; M_I (g mol^{-1}) is the molar mass of ^{131}I ; M_{Cs} (g mol^{-1}) is the molar mass of
 181 ^{137}Cs ; λ_I (s^{-1}) is the radioactive decay rate of ^{131}I ; λ_{Cs} (s^{-1}) is the radioactive decay rate of ^{137}Cs ;
 182 NA (mol^{-1}) is the Avogadro constant; V_m ($\text{m}^3 \text{mol}^{-1}$) is the molar volume of the air; and ρ_{air}
 183 (kg m^{-3}) is the air density.

184 Applying the ideal gas law to atmospheric air:

$$185 \quad pV_m = RT \quad (5)$$

186 Thus,

$$187 \quad V_m = \frac{RT}{p} = M_{\text{air}} \alpha_{\text{air}} \quad (6)$$

188 where M_{air} (kg mol^{-1}) is the molar mass of the air and α_{air} ($\text{m}^3 \text{kg}^{-1}$) is the specific volume of
 189 the air.

190 Based on the Eq. (3) and Eq. (4), we obtain the following equations,

$$191 \quad W_I = \frac{A_I M_{\text{air}} \alpha_{\text{air}}}{I_I NA} 10^6 \quad (7)$$

$$192 \quad W_{Cs} = \frac{A_{Cs} M_{Cs} \alpha_{\text{air}}}{I_{Cs} NA} 10^6 \quad (8)$$

193 In the advection-diffusion solver of WRF/Chem, we use W_I and W_{Cs} to calculate the transport
 194 of ^{131}I and ^{137}Cs respectively, and subsequently use A_I and A_{Cs} converted based on inversion of
 195 Eq. (7) and Eq. (8) for the outputs.

196

197 **2.3 Parameterizations of removal processes**

198 To simulate the transport and deposition of radionuclides more realistically, we added the

199 radioactive decay process into the advection-diffusion solver. To examine the performance of
200 different parameterizations in capturing the ground deposition of radionuclides, we improved
201 the default resistance method for dry deposition and added two new dry deposition
202 parameterization schemes: (1) the simple method and (2) the constant deposition velocity
203 method. Furthermore, we implement a parameterization based on the relative humidity for
204 wet deposition, in addition to the default WRF/Chem parameterization based on the
205 precipitation rate.

206

207 **2.3.1 Radioactive decay**

208 The radioactive decay is similar to a first-order chemical reaction. The **transient** air
209 concentration of a radioactive material, A , can be described as:

$$210 \quad A = A_0 e^{-\lambda t} \quad (9)$$

211 where A_0 represents the air concentration at $t = 0$. The radioactive decay rates are taken from
212 [IAEA \(2001\)](#) (International Atomic Energy Agency): $\lambda_I = 9.98 \times 10^{-7} \text{ (s}^{-1}\text{)}$ and $\lambda_{Cs} = 7.33 \times$
213 $10^{-10} \text{ (s}^{-1}\text{)}$. Considering the low radioactive decay rate of ^{137}Cs (equivalent to a half-life of
214 about 30 years), its decay process is neglected in this study, while the radioactive decay of ^{131}I
215 is retained (half-life of about 8 days).

216

217 **2.3.2 Dry deposition**

218 As presented in ([Seinfeld and Pandis, 2006](#)), we assume that the dry deposition flux is
219 proportional to the local air concentration of the radionuclides at the lowest level of the
220 atmospheric model:

$$221 \quad F = -v_{\text{dep}} A \quad (10)$$

222 where v_{dep} is the dry deposition velocity. In this study, three different parameterizations of the
223 dry deposition velocity are tested.

224

225 a. The resistance method

226 Based on (Wesely, 1989), the dry deposition velocity for gases is described by three
227 characteristic resistances, as follows:

$$228 \quad v_{\text{dep}} = \frac{1}{r_a + r_b + r_s} \quad (11)$$

229 where r_a is the aerodynamic resistance; r_b is the quasi-laminar layer (viscous sublayer)
230 resistance; and r_s is the surface resistance (describing the resistance of the surface to the
231 uptake/absorption/adsorption of the gas). The parameterizations of these three resistances in
232 our study follows Brandt et al. (2002).

233 For particles, the surface resistance is neglected while the gravitational settling velocity is
234 considered instead. The deposition velocity for particles can be expressed as (Seinfeld and
235 Pandis, 2006):

$$236 \quad v_{\text{dep}} = u_{\text{grav}} + \frac{1}{r_a + r_b + r_a r_b u_{\text{grav}}}, \quad (12)$$

237 where u_{grav} is the gravitational settling velocity. According to (Brandt et al., 2002), the
238 gravitational settling velocity can be calculated from the Stokes equation (small particles in
239 the atmosphere experience a creeping flow, Reynolds number $\ll 1$, that appears to change in
240 time due to the larger scale turbulent eddies):

$$241 \quad u_{\text{grav}} = \frac{d_p^2 g (\rho_p - \rho) Cc}{18\nu} \quad (13)$$

242 where d_p is the particle diameter, g the acceleration of gravity, ρ_p the particle density (1.88 g
243 cm^{-3} for Cesium (Weast, 1988) and 3.5 g cm^{-3} for Iodine (Ristovski, 2006) (the units of the
244 particle density are converted to kg m^{-3} for use in WRF/Chem)), ρ the density of air, ν the
245 kinematic viscosity of air ($1.5 \times 10^{-5} \text{ m}^2 \text{ s}^{-1}$) and Cc is the Cunningham correction factor
246 given by (Brandt et al., 2002).

247
$$C_c = 1 + \frac{\lambda_{\text{air}}}{d_p} \left(2.514 + 0.80 \exp \left(-\frac{0.55 d_p}{\lambda_{\text{air}}} \right) \right) \quad (14)$$

248 where $\lambda_{\text{air}} = 6.53 \times 10^{-8}$ m is the mean free path at standard temperature and pressure.

249 For particles, it can be seen in Eq. (12) that the dry deposition velocity not only depends on
 250 the gravitational settling velocity u_{grav} , but also depends on the aerodynamic resistance r_a and
 251 the quasi-laminar layer resistance r_b , all of which are affected by the particle density ρ_p .
 252 However, when taken together, the particle density does not affect the simulation results of the
 253 dry deposition considerably.

254

255 b. The simple parameterization

256 According to (Brandt et al., 2002), the dry deposition velocity can be calculated by a simple
 257 parameterization based on the friction velocity and the Obukhov length:

258
$$v_{\text{dep}} = \frac{u_*}{a}, \quad L > 0 \quad : \text{ stable conditions}$$

$$v_{\text{dep}} = \frac{u_*}{a} \left(1 + \left(\frac{300}{-L} \right)^{2/3} \right), \quad L < 0 \quad : \text{ unstable conditions} \quad (15)$$

259 where u_* is the friction velocity and L is the Obukhov length (Stull, 1988); a is a constant,
 260 which for low vegetation is set to 500 and for forests to 100 (Brandt et al., 2002).

261

262 c. The constant deposition velocity method

263 In this parameterization, the dry deposition velocity is simply a constant. We use typical
 264 values for ^{131}I and ^{137}Cs that are found in the literature: the dry deposition velocity of
 265 gas-phase ^{131}I is 0.5 (cm s^{-1}) (Baklanov and Sorensen, 2001), the dry deposition velocity of
 266 particulate ^{131}I is 0.1 (cm s^{-1}) (Baklanov and Sorensen, 2001) and the dry deposition velocity
 267 of ^{137}Cs is 0.05 (cm s^{-1}) (Maryon et al., 1991) (the units of all deposition velocities are
 268 converted to m s^{-1} for use in WRF/Chem).

269

270 In this study, the accumulated dry deposition at each location is calculated. The decay process
271 of radionuclides after they reach the ground surface follows the same radioactive decay rate.
272 In addition, additional decay can occur due to soil activity; this additional decay can be
273 represented by a constant λ_s , which has the same units as the radioactive decay (s^{-1}). Thus, the
274 accumulated ground deposition can be computed using the following equation,

$$275 \quad D_{gr}(t) = \int_{t_0}^t -v_{dep} A e^{-(\lambda + \lambda_s)t} dt \quad (16)$$

276 where D_{gr} ($Bq m^{-2}$) is the accumulated ground deposition, t_0 the initial time of deposition, t the
277 duration after deposition, and λ the (first-order) radioactive decay rate (s^{-1}). In this study, the
278 reduction rate due to soil activity λ_s of ^{131}I and ^{137}Cs are specified as 0 and 1.62×10^{-9} (s^{-1})
279 respectively (IAEA, 2001).

280

281 2.3.3 Wet deposition

282 a. The parameterization based on precipitation rate

283 Following Sportisse (2007), the wet deposition rate is described as:

$$284 \quad L^s = a p_0^b \quad (17)$$

285 where p_0 is the rain intensity ($mm h^{-1}$); a and b are the parameters for specified radionuclides.
286 In this study, we set $a = 4 \times 10^{-5}$ and $b = 0.6$ for gaseous ^{131}I (Sportisse (2007), $a = 7 \times 10^{-5}$
287 and $b = 0.69$ for particulate ^{131}I (Jylha, 1991), and $a = 8 \times 10^{-5}$ and $b = 0.8$ for ^{137}Cs
288 (Baklanov and Sorensen, 2001).

289

290 b. The parameterization based on relative humidity

291 The parameterization based on the relative humidity (RH) is another scheme for calculating

292 the wet deposition rate (Pudykiewicz, 1989):

$$\begin{aligned} \Lambda^s &= 0, \quad RH < RH_t \\ \Lambda^s &= 3.5 \times 10^{-5} \left(\frac{RH - RH_t}{RH_s - RH_t} \right), \quad RH \geq RH_t \end{aligned} \quad (18)$$

294 where RH_t (= 80%) is the threshold value of the relative humidity and RH_s (= 100%) is the
295 saturation value.

296 Similar to the accumulated dry deposition, in this study, the accumulated wet deposition is
297 also calculated. The same constants for the increased decay rates due to soil activity of ^{131}I
298 and ^{137}Cs are used for wet and dry deposition. In addition, the wet deposition rate Λ^s is
299 height-dependent in this RH -based model. Following (Seinfeld and Pandis, 2006), the wet
300 ground deposition can be calculated following:

$$301 \quad W_{\text{gr}}(t) = \int_{t_0}^t \int_0^h \Lambda^s(z) A(z) e^{-(\lambda + \lambda_s)t} dz dt, \quad (19)$$

302 where W_{gr} (Bq m^{-2}) is the wet ground deposition and h is the height of the domain.

303

304 2.4 WRF configurations

305 The simulations are performed using 3 nested domains with horizontal resolutions of 9 km, 3
306 km, and 1 km for domain 1, domain 2, and domain 3, respectively (see Fig. 2). Domain 1 and
307 Domain 2 are centered at 37.5 N, 141.0 E with 160 grid points in both the north-south
308 direction and the east-west direction. Domain 1 nearly covers the whole of Japan and Domain
309 2 covers most of the Tohoku region and the Kanto region where observational stations are
310 located. The innermost domain has 160×160 grids and is centered at 36.9 N, 140.4 E.

311 The simulation uses 27 vertical levels for all domains, with the highest level at the 10000 Pa
312 isobaric surface (WRF uses terrain following pressure coordinates in the vertical direction).

313 The emissions are only released at the lowest level. The Global Forecasting System (GFS)
314 reanalysis, with a $0.5^\circ \times 0.5^\circ$ horizontal resolution, is used for initial and boundary conditions.

315 The simulation period starts from 00 UTC March 11 and ends at 00 UTC March 31, 2011

316 with 1 hour output interval. In this study, we conduct one reference case simulation (REF) and
317 12 sensitivity simulations as summarized in [Table 1](#). One-way nesting is used for all
318 simulations. Other physics schemes that are not changed include: (1) the Rapid **Radiative**
319 **Transfer Model** for long wave radiation, (2) the Dudhia scheme for short wave radiation, (3)
320 the Yonsei University scheme for the planetary boundary layer, (4) the Noah Land Surface
321 Model for non-urban land surface physics, (5) the single-layer urban canopy model for urban
322 surface physics, (6) the New Grell scheme for cumulus parameterization (in this study,
323 cumulus parameterization is only used for the domain 1; the other domains have fine
324 resolutions that should allow them to resolve shallow convection).

325

326 **2.4.1 Reference simulation**

327 Simple aerosol treatment, using an aerosol scheme in which no direct or indirect effects are
328 considered, is used. In the reference case, the 2D Smagorinsky scheme is used for horizontal
329 diffusion and the WSM 6 (**WRF Single-Moment 6-class**) scheme is used for the microphysics.
330 The resistance method is used for parameterizing dry deposition and the parameterization
331 based on precipitation rate is used for wet deposition. The partitioning of ^{131}I at the source is
332 chosen to be 80% gas as recommended in several studies ([Korsakissok et al., 2013](#); [Morino et](#)
333 [al., 2011](#)). Moreover, in the reference case, the size distribution of particulate radionuclides is
334 not taken into account: all particulate radionuclides have the same size, which is the average
335 value. **The** average size of ^{131}I and ^{137}Cs are chosen to be 0.48 and 0.67 μm , respectively
336 ([Kaneyasu et al., 2012](#); [Sportisse, 2007](#)).

337

338 **2.4.2 Sensitivity studies**

339 As shown in [Table 1](#), a variety of sensitivity simulations are carried out to evaluate the impact
340 of different physics/parameterizations on the atmospheric transport and ground deposition of
341 radionuclides. In case 2, the emission rate estimated by TEPCO is used to assess the

342 uncertainty in the emission source term and its impact. In cases 3 and 4, two different
 343 microphysics schemes, the Goddard scheme and the Thompson scheme, are used to examine
 344 the impact of microphysics schemes on rainfall and on the modeling of transport and
 345 deposition of radionuclides. In case 5, the horizontal diffusion scheme is chosen to be the 1.5
 346 order TKE scheme, as compared to the Smagorinsky scheme that is used in the reference case.
 347 Cases 6, 7, 8 and 9 are designed to assess the sensitivity of simulated results of ^{131}I to the gas
 348 partitioning, with the gaseous fraction of ^{131}I decreasing from 100% to 0%. In case 10, the
 349 **log-normal** size distribution of ^{137}Cs is considered; the average size remains $0.67\ \mu\text{m}$ but the
 350 standard deviation is set to $1.3\ \mu\text{m}$ (Kaneyasu et al., 2012). As compared to the reference case,
 351 cases 11 and 12 use the simple parameterization method and the constant deposition velocity
 352 method, respectively, to parameterize dry deposition; case 13 uses the parameterization based
 353 on relative humidity for wet deposition.

354 Errors including Percentage Bias (PBIAS), Percentage Root Mean Square Error (PRMSE)
 355 and Mean Bias Error (MBE) are used to evaluate the model performance and compare the
 356 results from different sensitivity cases. PBIAS and PRMSE are used for wind speed,
 357 precipitation and total deposition; while MBE is only used for evaluating the wind direction
 358 for which percentage errors are not adequate (e.g. when the observed value is 1° and the
 359 modeled value is 359° ; the PBIAS is -35800% ; when the observed value is 357° and the
 360 modeled value is 359° ; the PBIAS is -0.57% ; however the absolute errors of the wind
 361 direction under these two conditions are both 2°).

362 PBIAS, PRMSE and MBE are defined as follows:

$$363 \quad \text{PBIAS} = \frac{\frac{1}{n} \sum_{i=1}^n (O_i - M_i)}{\frac{1}{n} \sum_{i=1}^n O_i} \times 100 \quad (20)$$

$$364 \quad \text{PRMSE} = \frac{\sqrt{\frac{1}{n} \sum_{i=1}^n (O_i - M_i)^2}}{\frac{1}{n} \sum_{i=1}^n O_i} \times 100 \quad (21)$$

365
$$\text{MBE} = \frac{1}{n} \sum_{i=1}^n (O_i - M_i) \quad (22)$$

366 where O_i represents the observed value and M_i represents the modeled value.

367

368 **2.5 Observational datasets**

369 Hourly wind speed, wind direction¹ and rainfall² data are obtained from National Climatic
370 Data Center (NCDC) at stations YAMAGATA, CHIBA, TOKYO, ONAHAMA, NIIGATA,
371 MAEBASHI, SENDAI and ISHINOMAKI. These data are used to assess the WRF-simulated
372 wind and rainfall fields. Daily total deposition of ¹³¹I and ¹³⁷Cs are measured by bulk samplers
373 over 46 stations, which are provided by Ministry of Education, Culture, Sports, Science and
374 Technology (MEXT)³. In this study, we only select 7 of the 46 stations to evaluate the model
375 since most of the stations do not have available data covering the period from March 18 to
376 March 31 (all of the 46 stations do not have available data before March 18). The 7 stations
377 are YAMAGATA, IBARAKI, TOCHIGI, GUNMA, SAITAMA, CHIBA and TOKYO.

378

379 **3 Results and Discussion**

380 This section is organized in the following way: in Section 3.1, the simulated wind and rainfall
381 fields are evaluated, and their impact on the atmospheric transport and ground deposition of
382 radionuclides is assessed. Section 3.2 analyzes the contributions of dry and wet deposition to
383 total deposition and examines the sensitivity of ground deposition to different
384 parameterizations of dry and wet deposition. Section 3.3 examines the sensitivity of ground
385 deposition to the different characteristics of the emission rate, the gas partitioning of ¹³¹I and
386 the size distribution of ¹³⁷Cs.

387

¹ <http://cd0.ncdc.noaa.gov/pls/plclimprod/poemain.cdobystn?dataset=DS3505&StnList=47409099999>

² <http://www.ncdc.noaa.gov/cdo-web/datasets/GHCND/stations/GHCND:JA000047409/detail>

³ <http://www.mext.go.jp/english/incident/1307872.htm>.

388 **3.1 Meteorological fields and their influence on deposition of radionuclides**

389 This section **evaluates** the WRF-simulated wind and rainfall fields using observational data at
390 various locations. The impact of wind and rainfall on the atmospheric transport and ground
391 deposition of radionuclides is also examined. In particular, the sensitivity of deposition to
392 different microphysical parameterizations and horizontal diffusion schemes in WRF is
393 investigated.

394

395 **3.1.1 Evaluation of WRF-simulated wind and rainfall fields and their sensitivity** 396 **to the horizontal diffusion and microphysics schemes**

397 WRF-simulated wind speed and direction at 10 m in the reference case (REF) from domain 2
398 are compared to observed data over 8 stations in Japan and the results are shown in [Fig. 3](#) and
399 [Fig. 4](#). **The** wind fields simulated by WRF show a good agreement with the observations at
400 most of the stations such as CHIBA, SENDAI and ISHINOMAKI. Nevertheless, WRF
401 significantly overestimated the wind speed at YAMAGATA during the whole simulation
402 period, **with correspondingly large biases in wind direction at that station.**

403 The biases in the WRF-simulated wind fields are quantified using PBIAS, PRMSE, and MBE
404 as introduced in Section 2 ([Table 2](#)). **These** statistics are also calculated for the case using the
405 1.5-order TKE horizontal diffusion scheme (DIF2) in addition to the reference case (REF). **In**
406 **the Smagorinsky scheme, the horizontal diffusion coefficient K is diagnosed from the**
407 **horizontal strain rate magnitude, while in the 1.5 TKE scheme a prognostic equation for**
408 **turbulent kinetic energy (TKE) is used, and K is based on the TKE. The vertical diffusion**
409 **coefficient for both cases are computed by the PBL scheme.** The values of PBIAS, PRMSE
410 and MBE are quite close for both cases. However, as shall be seen later, the subtle differences
411 in the wind fields generated by using two different horizontal diffusion schemes can result in
412 significant differences in the ground deposition of radionuclides. It is clear that the PBIAS for
413 wind speed at CHIBA, SENDAI and ISHINOMAKI are lower than 7% and the PRMSE at
414 these 3 stations are also lower than at other stations. The PBIAS and PRMSE for wind speed

415 at YAMAGATA are significantly higher than those at other stations, which is in agreement
416 with Fig. 3 and Fig. 4. As for the wind direction, the MBE at CHIBA, NIIGATA and
417 ISHINOMAKI are lower than 30 degrees. Nevertheless, at YAMAGATA, the MBE of wind
418 direction is about 50 degrees for both diffusion schemes. The YAMAGATA station is located
419 in an area surrounded by mountains, thus the large biases in the simulated wind speed and
420 wind direction at YAMAGATA may be due to the coarse grid resolution (3 km, domain 2) that
421 is unable to resolve the subgrid-scale topography.

422 The simulated daily precipitation rate in the reference case (REF) is also compared to
423 observational data at the 8 stations and the results are shown in Fig. 5. The WRF-simulated
424 daily precipitation is in good agreement with the observations except at YAMAGATA,
425 SENDAI, and ISHINOMAKI. At YAMAGATA, the WRF-simulated rainfall is a day ahead of
426 the observed rainfall and the maximum rainfall rate is significantly underestimated by WRF.
427 At SENDAI and ISHINOMAKI, the maximum rainfall rate is not captured well by WRF, but
428 the timing is almost correct. In order to examine the sensitivity of simulated rainfall to
429 different microphysical parameterizations, the precipitation patterns generated from 3
430 different microphysics schemes are compared in Fig. 6 (REF with WSM 6, MP2 with
431 Goddard, MP3 with Thompson). The left panels show the daily precipitation on March 21 and
432 the right panels show the accumulated precipitation from March 11 to 31 over domain 2. Both
433 the daily precipitation on March 21 and the accumulated precipitations show quite similar
434 patterns overall, but there are differences observed among the three cases with the different
435 microphysical parameterizations. For example, in the left panels, around 35.5N - 36N, 138.5E
436 - 140.5E (as outlined by the black circles in Fig. 6) where the maximum precipitation occurs,
437 the area with high precipitation values (> 20 mm) in case REF or MP2 is significantly larger
438 than that in case MP3.

439 The errors associated with the simulated rainfall fields are quantified by PBIAS and PRMSE,
440 as shown in Table 3. It is clear that the PBIAS values at most of the stations are lower than
441 30% while the PRMSE values are about 200%; this indicates that although there are large

442 biases associated with the time series of rainfall, a significant fraction of these biases are
443 related to timing and the averaged or the accumulated rainfall (which cancel the timing errors
444 and are hence more accurately represented by PBIAS) are fairly well captured by WRF. This
445 is not the case at station ISHINOMAKI where the values of PRMSE and PBIAS are
446 extremely high. This is because the observational data at this station is only available after
447 March 20 when the precipitation is significantly overestimated by WRF simulations (see Fig.
448 5). The comparison among the three microphysical schemes shows that case REF yields the
449 least PBIAS at CHIBA, NIIGATA, MAEBASHI, SENDAI, and ISHINOMAKI. In particular,
450 the PBIAS from case REF are significantly smaller than those from cases MP2 and MP3 at
451 NIIGATA, MAEBASHI, and SENDAI. At TOKYO, the PBIAS from case REF is comparable
452 to that from case MP2, while at ONAHAMA it is comparable to that from case MP3. Only at
453 YAMAGATA does the REF case produce the largest PBIAS; nonetheless, all of the three
454 microphysical schemes yield very small PBIAS at YAMAGATA. As such, it can be concluded
455 that the WSM 6 microphysical scheme used in case REF performs the best among the three
456 schemes examined here, at least for this study.

457

458 **3.1.2 Influence of wind and rainfall on the transport and deposition of** 459 **radionuclides**

460 In order to illustrate the impact of wind fields on the atmospheric transport of radionuclides,
461 the concentration maps of ^{131}I at the lowest level of the atmospheric model at four different
462 times (i.e., 00, 06, 12, 18 UTC) on March 21 are illustrated in the upper four panels of Fig. 7,
463 along with wind vector field. At 00 UTC, the transport of the radionuclides from FDNPP is
464 driven by northerly winds (towards the south). One can also notice the large concentrations to
465 the east, over the Pacific Ocean, and to the north of FDNPP at 00 UTC that are probably the
466 remnants of pervious northeastward winds. The transport direction changes with wind and
467 becomes northeasterly (towards the southwest, from the source to the Kanto region) from 12
468 UTC to 18 UTC gradually. The bottom panels of Fig. 7 shows the accumulated daily dry and

469 wet deposition on March 21. As suggested by the concentration maps, the deposition is
470 highest in the Kanto region that lies southwest of FDNPP. Dry deposition is small compared
471 with wet deposition and the two depositions display different spatial patterns. In this REF case,
472 the parameterization of wet deposition is based on precipitation. As shown in Fig.6, there is a
473 large amount of precipitation in the southwest area and hence the wet deposition is also high
474 over this area. Thus, it is evident that the ground deposition, including dry and wet deposition,
475 is influenced by both wind and rainfall.

476 The total deposition from cases using different horizontal diffusion schemes and
477 microphysical schemes are compared in Fig. 8, where we show the daily total deposition at
478 stations YAMAGATA and CHIBA as two examples. The results of both ^{131}I and ^{137}Cs indicate
479 that the difference between REF and DIF2 is small at CHIBA but large at YAMAGATA. At
480 YAMAGATA, the total daily deposition of both ^{131}I and ^{137}Cs in REF is only about half of
481 that in DIF2 on March 20, while it is slightly higher in DIF2 than that in REF on March 22
482 and 25. Much larger differences are seen among different microphysics schemes at both
483 CHIBA and YAMAGATA. For example, at YAMAGATA on March 20, the deposition of
484 ^{137}Cs simulated by REF is about 3.9 kBq/m^2 and it is close to the observed value; while in
485 MP2 and MP3, the amounts of deposition are 2.2 and 7.9 kBq/m^2 , respectively. Fig. 8 also
486 illustrates that the ground deposition of radionuclides are sensitive to both horizontal diffusion
487 schemes and microphysical schemes. This however does not contradict our previous finding
488 that at the 8 stations with measurements of wind speed and wind directions, the biases
489 generated by the two cases using different horizontal diffusion schemes are relatively similar.
490 **The** daily accumulated ground deposition at one particular location is in fact affected by
491 winds over the upwind fetch as well as turbulence levels at a given location. **Hence, despite**
492 the fact biases seen in the wind fields over the 8 stations are similar for the two horizontal
493 diffusion schemes, the turbulence and upstream winds in the two cases are not necessarily
494 similar. Furthermore, small differences in wind fields can generate relatively larger
495 differences in precipitation **patterns and locations** and thus influence wet deposition. As such,
496 subtle differences seen in the wind field in Table 2 might result in significant differences in

497 the ground deposition depending on the sensitivity of ground deposition and precipitation to
498 the wind field.

499 The PBIAS and PRMSE of total deposition of ^{131}I and ^{137}Cs with different horizontal
500 diffusion schemes and microphysics schemes are presented in Table 4 and Table 5,
501 respectively. In order to evaluate the performance of different schemes in a quantitative and
502 consistent way, a ranking system is proposed. At each station, a local rank (LR) is assigned to
503 each scheme. The scheme with the smallest error has rank 1 and the scheme with the second
504 smallest error has rank 2, etc. Then a global rank (GR) is calculated by summing the local
505 rank of each scheme over all stations. Finally, the global rank calculated with PBIAS and that
506 calculated with PRMSE are summed up to yield a summed global rank (SR), which is used to
507 compare the performance of different parameterization schemes. A scheme with the smallest
508 SR performs the best among all the schemes that it is compared against. As shown in Table 4,
509 the errors in case REF are close to those in case DIF2. However, the global ranks inferred
510 from PBIAS and PRMSE are lower in case DIF2 than those in case REF for both ^{131}I and
511 ^{137}Cs , indicating that, globally, using the 1.5 order TKE scheme predicts the ground
512 deposition better than using the horizontal Smagorinsky scheme.

513 Table 5 shows the errors in simulated total daily depositions of ^{131}I and ^{137}Cs with different
514 microphysics schemes. It is shown that PBIAS in all 3 cases are below 100% over the 7
515 stations except that of ^{137}Cs at TOCHIGI and GUNMA. However, most of the PRMSE values
516 of ^{131}I and ^{137}Cs are larger than 100%, especially in TOCHIGI and GUNMA where the
517 PRMSE of ^{137}Cs is over 1200% in case MP3 and at least over 400% in the other two cases,
518 suggesting that the model cannot capture the total daily deposition of ^{137}Cs at these 2 stations.
519 Case REF has the lowest global rank based on both PBIAS and PRMSE for both ^{131}I and
520 ^{137}Cs , which suggests that the microphysics scheme WSM 6 can better predict the total daily
521 deposition than the Goddard scheme and the Thompson scheme. The much higher values of
522 PRMSE compared to PBIAS indicates that a significant component of the errors are due to
523 time shifts in the deposition patterns. Overestimations and underestimations of deposition at

524 various times partially cancel each other in PBIAS, but not in PRMSE. Overall however,
525 since one is interested in total deposition even if the timing is not very accurate, PBIAS might
526 be a better measure of the ability of WRF to simulate the environmental impact of
527 radionuclides deposition from the Fukushima accident.

528

529 **3.2 Dry and wet deposition**

530 This section examines the contributions of dry and wet deposition to total deposition, and
531 examines the sensitivity of ground deposition to different parameterizations of dry and wet
532 deposition processes.

533

534 **3.2.1 Contributions of dry and wet deposition to total deposition**

535 Simulated total daily depositions of ^{131}I and ^{137}Cs from March 11 to 31 at various locations
536 indicate that the total daily depositions of ^{131}I and ^{137}Cs are significant at all of the 7 stations
537 during two periods: from March 15 to 16 (not shown) and from March 20 to 23. These
538 periods with high total daily depositions correspond to periods with high emission rates from
539 the source (Fig. 1). Since there is no observational data for ground deposition before March
540 18, the following analyses will focus on the period from March 18 to March 31, with
541 maximum total daily depositions occurring from March 20 to 23.

542 Comparisons between simulated total daily depositions of ^{131}I and ^{137}Cs and observational
543 data are shown in Fig. 9. During the period from March 18 to 31, simulated total daily
544 depositions generally follow the pattern observed in the measurements; however, the
545 simulations significantly underestimate the observed deposition peak of ^{131}I around March 20
546 to 22 at most stations. As for ^{137}Cs , the total daily depositions are overestimated at TOCHIGI,
547 GUNMA and SAITAMA and underestimated at YAMAGATA, IBARAKI and CHIBA, which
548 is consistent with the results reported by Morino et al. (2011) using a CMAQ model coupled
549 with WRF in their study. Morino et al. (2011) indicated that the deposition rates of ^{137}Cs at

550 IBARAKI were underestimated, but those at the TOCHIGI, GUNMA and SAITAMA were
551 overestimated by their model. From Fig. 9, it is clear that the total deposition is dominated by
552 wet deposition over all of the stations for both ^{131}I and ^{137}Cs . The exceptions are TOCHIGI
553 where the dry deposition of ^{131}I contributes about half of the total deposition on March 21 and
554 YAMAGATA where the dry deposition of ^{131}I is about 1/3 of the total deposition on March
555 20.

556 Figure 10 examines the spatial distribution of accumulated dry and wet depositions of ^{131}I and
557 ^{137}Cs over domain 2 from March 11 to March 31. For ^{131}I , the area with dry deposition over
558 100 kBq/m^2 is concentrated near the source and is much smaller than the area with wet
559 deposition over 100 kBq/m^2 . The spatial distribution of the accumulated wet deposition does
560 not exactly follow that of the accumulated precipitation that was shown in Fig. 6, suggesting
561 that other factors such as wind, concentration fields, and the emission rate also play an
562 important role in determining the distribution of wet deposition. The wet deposition of ^{131}I in
563 the northeast area is much larger than the dry deposition, while along the east coast, the dry
564 deposition is sometimes higher than the wet deposition. This implies that wet deposition does
565 not necessarily dominate over dry deposition at all locations.

566 As for ^{137}Cs , the pattern of dry deposition is quite different from that of ^{131}I ; and most of the
567 areas have values lower than 5 kBq m^{-2} . The reason for these differences is that the dry
568 deposition parameterizations depend on resistances that are quite different between ^{131}I and
569 ^{137}Cs , and the dry deposition velocity of ^{137}Cs is much smaller than that of gaseous ^{131}I . The
570 wet deposition, on the other hand, shows a similar pattern to that of ^{131}I , but the values are
571 slightly lower than those of ^{131}I in some areas such as north of Fukushima. These comparisons
572 imply that the dry and wet depositions of different radionuclides are affected by wind and
573 rainfall in different ways.

574

575 **3.2.2 Sensitivity of ground deposition to the parameterizations of dry and wet**
576 **deposition**

577 To assess the sensitivity of total daily depositions to different dry and wet deposition
578 parameterization schemes, the results from cases REF (with the resistance method for dry
579 deposition, and with the parameterization based on precipitation rate for wet deposition),
580 DRY2 (with the simple parameterization method for dry deposition), DRY3 (with the constant
581 dry deposition velocity) and WET2 (with the parameterization based on relative humidity) are
582 compared. In Fig. 11 the total daily depositions at stations IBARAKI and TOCHIGI are
583 shown as examples. The deposition from case REF and DRY2 are nearly the same during the
584 whole period. Except for ^{131}I at TOCHIGI, the deposition from case DRY3 is also very close
585 to that in case REF and DRY2. The reason why different dry deposition parameterizations do
586 not alter the total daily deposition of ^{131}I at station IBARAKI and those of ^{137}Cs at stations
587 IBARAKI and TOCHIGI significantly is that they are dominated by wet deposition. At
588 TOCHIGI, the dry deposition of ^{131}I contributes nearly the same to the total deposition as wet
589 deposition, as can be seen from Fig. 9. As such, the total deposition of ^{131}I at TOCHIGI is
590 sensitive to the dry deposition parameterizations in WRF. Nevertheless, the results from REF
591 and DRY2 are still very close for ^{131}I at TOCHIGI, suggesting that the resistance method and
592 the simple parameterization yield similar dry daily depositions.

593 As shown in Fig. 11, the total daily depositions in case WET2 (parameterization based on
594 relative humidity) are significantly lower than those in case REF for both ^{131}I and ^{137}Cs at
595 these two stations. For example, in TOCHIGI, the deposition of ^{137}Cs from case WET2 is only
596 half of that from case REF. Thus, the total deposition is more sensitive to the choice of the wet
597 deposition scheme than to the choice of the dry deposition scheme, which is due to the fact
598 that the total depositions at these two stations are dominated by wet depositions. However, the
599 TOCHIGI, the comparison of the different runs does indicate that the parameterizations of the
600 two methods of deposition have comparable influence on the results when their relative
601 contributions to total deposition are comparable.

602 The PBIAS and PRMSE of total daily depositions of ^{131}I and ^{137}Cs with different dry and wet
603 deposition parameterizations are shown in Table 6 and Table 7, respectively. The PBIAS and
604 PRMSE in REF, DRY2 and DRY3 are quite similar, suggesting that the total daily deposition
605 for this accident is not sensitive to the choice of the dry deposition scheme, **again** we reiterate
606 that this can be different for other cases where the dry deposition contributes a larger fraction
607 of the total deposition. This is in agreement with Fig. 11. To select the “best” dry deposition
608 scheme, the sum of global rank (SR) is compared. Case REF **and Case DRY2 have** the lowest
609 SR for ^{131}I while case DRY3 has the lowest SR for ^{137}Cs , indicating that the resistance method
610 **and the simple parameterization have** the best performance in capturing the total deposition of
611 ^{131}I while the method with **a** constant dry deposition velocity (0.05 cm s^{-1}) has the best
612 performance in capturing the total deposition of ^{137}Cs , which essentially precludes making
613 any robust inferences or recommendation about the choice of the optimal dry deposition
614 model.

615 The PBIAS and PRMSE in case WET2 are of the same magnitude over most of stations as
616 those in case REF. As for ^{131}I , case REF has the lowest SR; while for ^{137}Cs , **case WET2 has**
617 **the lowest SR**. These results suggest that using the wet deposition parameterization based on
618 precipitation rate can predict the total daily deposition of ^{131}I **better**, while for capturing the
619 total daily deposition of ^{137}Cs , **using the wet deposition parameterizations based on relative**
620 **humidity has a better performance.**

621

622 **3.3 The influence of emission rates and characteristics**

623 This section examines the sensitivity of ground deposition of ^{131}I and ^{137}Cs to the different
624 characteristics of the emission source, including the emission rate, the gas partitioning of ^{131}I ,
625 and the size distributions of ^{137}Cs . Fig. 12 shows the WRF-simulated and observed daily
626 depositions of ^{131}I and ^{137}Cs at stations GUNMA and TOKYO. As can be seen in the figure,
627 there are significant differences in the daily depositions of ^{131}I and ^{137}Cs at these two stations
628 between the case using the emission rate estimated by JAEA and the case using emission rate

629 estimated by TEPCO. The simulated depositions using the emission rate estimate by JAEA
630 (REF) are lower than those from the case using emission rate by TEPCO (EM2) on March 19
631 – 23 when deposition occurs at these two stations. In particular, at GUNMA, the deposition of
632 ^{131}I in EM2 is about 15 times that in REF and the deposition of ^{137}Cs in EM2 is about 4 times
633 of that in REF. Fig. 13 depicts the spatial patterns of the accumulated depositions of ^{131}I and
634 ^{137}Cs from REF and EM2 from March 11 to 31. For ^{131}I , the area with accumulated deposition
635 exceeding 100 kBq/m^2 is much larger in EM2 than that in REF, covering nearly half of domain
636 2 over the southeast area. For ^{137}Cs , in the west of FDNPP (37 N - 38 N, 139.5E - 140.5E),
637 REF produces higher depositions than EM2. The above results clearly demonstrate that the
638 emission rates, and their temporal distributions, have a major influence on ground deposition
639 of radionuclides. Temporal variability is important since it interacts with changes in wind
640 speed and direction to result in the concentration maps that produce the deposition maps.

641 The PBIAS and PRMSE of total daily depositions of ^{131}I and ^{137}Cs with different emission
642 rates are shown in Table 8. It is evident that the PBIAS and PRMSE of the total daily
643 depositions of ^{131}I and ^{137}Cs in case EM2 are significantly higher than those in case REF over
644 most of the stations, indicating that case REF better reproduces the observations. This is also
645 reflected by the lower SR value of case REF. Morino et al. (2013) used different emission
646 datasets in their CMAQ model simulation for the same accident and also reported that the
647 emission rate estimated by TEPCO generally overestimated the observations, which agrees
648 with the results reported in this paper.

649 In addition to emission rates, the gas partitioning of ^{131}I and the size distribution of ^{137}Cs are
650 the two emission characteristics examined in our study. In the cases REF, GP2, GP3, GP4 and
651 GP5, the gaseous fraction of ^{131}I is defined as 80%, 100%, 60%, 30% and 0, respectively. As
652 shown in the top panels of Fig. 12, total daily depositions of ^{131}I increase as the gaseous
653 fraction decreases (i.e., as the fraction of particulate species increases from GP2 to GP5),
654 which is especially prominent at the station in TOKYO. This result indicates that the total
655 deposition of ^{131}I is sensitive to its gas partitioning at the source, which has high uncertainty

656 (Sportisse, 2007). The fact that total daily depositions increase as the gaseous fraction
657 decreases also suggests that for the same amount of radionuclides released from the source
658 (these two stations are considered far from the source), more particulate species can be
659 transported to the stations far away from the source than gaseous species. This is because that
660 gaseous ^{131}I has a larger dry deposition velocity than particulate ^{131}I ; as a result, larger
661 amounts of gaseous ^{131}I deposit within a smaller area around the source (at least according to
662 the deposition models used here). Hence, less gaseous ^{131}I is transported to areas that are far
663 away from the source. Apart from that, the change in the partitioning of ^{131}I over time is also
664 associated with a high uncertainty, which may influence the removal rates since the gas to
665 particle conversion of ^{131}I typically occurs on time scales from 2-3 weeks (Masson, 2011).

666 The PBIAS and PRMSE of total deposition of ^{131}I with different gaseous fractions are shown
667 in Table 9. The PBIAS suggests that the GP4 case with gaseous fraction of 30% gives the best
668 result, while the PRMSE indicates that the GP3 case with gaseous fraction of 60% yields the
669 best result. The two cases also have very close SR values (the SR of GP4 is 28 and that of
670 GP3 is 27). Since there was no simulations with intermediate gaseous fractions, the results
671 can only indicate that the optimal gaseous fractions of ^{131}I lies somewhere between 30% or
672 60% for the model setup in this study, which is also consistent with the result from the study
673 by Momoshima et al. (2012).

674 WRF-simulated total daily depositions of ^{137}Cs at the seven monitored stations using a
675 log-normal size distribution for ^{137}Cs emission (i.e., case SD2) are compared with those using
676 a constant particle size (i.e., case REF) in the bottom panels of Fig. 12. The results at
677 GUNMA and TOKYO indicate that the difference between REF and SD2 is small during the
678 period of March 18 – 30. The comparisons at the other 5 stations show similar results (not
679 shown here). Consequently, the total deposition of ^{137}Cs is not very sensitive to the size
680 distribution from the comparisons at these 7 stations. This is also consistent with the study by
681 Morino et al. (2013), in which the reference case and the sensitivity case have nearly the same
682 errors including FAC2, FAC10 (the proportions of simulated data that reproduce the

683 observations within a factor of 2 or 10, respectively) and the correlation coefficient between
684 the observed and simulated depositions.

685 The PBIAS and PRMSE of total deposition of ^{137}Cs with two size distributions are shown in
686 Table 10. As can be seen, the PBIAS and PRMSE values are similar in the two cases, which is
687 consistent with Fig. 12. The SR value in case SD2 (= 20) is slightly lower than that in case
688 REF (= 22), which indicates that the case with a log-normal distribution for the size of ^{137}Cs
689 in the emission has a slightly better performance than the case with uniform particle size of
690 ^{137}Cs .

691

692 **3.4 The assessment of the sensitivity of the total daily deposition to the model** 693 **physics and inputs**

694 To assess the sensitivity of the total daily deposition to all of the model physics and inputs, the
695 difference between the error in the reference case and that in specific sensitivity cases is
696 calculated and compared. Table 11 shows the averaged absolute value of the difference (AAD)
697 between the error in the reference case and that in different sensitivity cases (e.g. the AAD for
698 PBIAS of ^{131}I between REF and EM2 is 172%). AAD is defined as:

$$699 \quad \text{AAD} = \left(\sum_{i=1}^n |Error_{\text{REF}} - Error_{\text{SENS}}(i)| \right) / n \quad (23)$$

700 where $Error_{\text{REF}}$ is the error in the reference case, $Error_{\text{SENS}}$ is the error in the specific
701 sensitivity case, i is the index of the observational station and n is total number of the stations,
702 here $n = 7$.

703 In order to compare the sensitivity of the total daily deposition to all of the model physics and
704 inputs, the sensitivity is divided into 3 groups based on AAD. If $\text{AAD} > 40\%$, the sensitivity is
705 defined to ‘very sensitive’, if $\text{AAD} > 10\%$ and $< 40\%$, the sensitivity is defined to ‘moderately
706 sensitive’, while if $\text{AAD} < 10\%$, the sensitivity is defined to ‘not sensitive’.

707 It can be seen that the AAD in terms of both PBIAS and PRMSE for both ^{131}I and ^{137}Cs is
708 larger than 100% for REF (with emission estimated from JAEA) – EM2 (with emission
709 estimated from TEPCO), thus the total daily deposition is very sensitive to the imposed
710 emission rate. Based on AAD, we can also conclude that for ^{131}I , the total daily deposition is
711 moderately sensitive to the microphysics schemes, the horizontal diffusion schemes, gas
712 partitioning and wet deposition parameterizations, and the total daily deposition is not
713 sensitive to the dry deposition parameterization. For ^{137}Cs , almost all of values of AAD for
714 REF-MP2, REF-MP3 and REF-WET2 are larger than 40%, so the total daily deposition is
715 also very sensitive to the microphysics schemes and wet deposition parameterizations, and it
716 is moderately sensitive to the horizontal diffusion schemes and the size distribution, but it is
717 not sensitive to the dry deposition parameterization.

718

719 **4 Conclusions**

720 This paper focuses on the atmospheric transport and ground deposition of radionuclides
721 following the Fukushima Daiichi accident using the WRF/Chem model and observational data.
722 The sensitivity of WRF-simulated results to a variety of parameters, including microphysics
723 schemes, horizontal diffusion schemes, parameterizations for dry deposition and wet
724 deposition, the emission rate, the gas partitioning of ^{131}I , and the size distribution of ^{137}Cs in
725 the emission is examined. The simulated meteorological fields such as wind speed, wind
726 direction, and precipitation are evaluated by comparing to observations; the simulated total
727 daily depositions are also compared to measurements. The percent bias (PBIAS) and percent
728 mean square error (PRMSE) are used to assess the errors in the simulated results; the sum of
729 the global rank (SR), which is based on the calculated PBIAS and PRMSE, is then used to
730 identify the schemes that perform the best. The averaged absolute value of the difference
731 (AAD) between the error in the reference case and that in different sensitivity tests is used to
732 assess the sensitivity of the simulated total daily depositions to all model physics and inputs.

733 The main conclusions, which are linked to questions 1 to 4 that we raise in the introduction,

734 are:

735 (1) The wind fields are overall well reproduced by WRF. The wind speed and wind direction
736 simulated using the Smagorinsky horizontal diffusion scheme (REF) and those using the 1.5
737 order TKE horizontal diffusion scheme (DIF2) yield similar results. However, the subtle
738 differences in the wind fields still result in a significant difference in the ground deposition of
739 radionuclides (e.g. the AAD for PRMSE of wind speed between REF and DIF2 is only 1.76%
740 calculated based on Table 2 and Eq. (23); however, the AAD for PRMSE of the deposition of
741 ^{131}I between the same two simulations is 17% and that of ^{137}Cs is 36% as shown in Table 11).
742 Based on SR, simulations using the 1.5 order TKE scheme predicted the ground deposition
743 better than those using the horizontal Smagorinsky scheme. The averaged or the accumulated
744 rainfall was fairly well captured by WRF, but the maximum rainfall rate was not as accurately
745 predicted in the sensitivity cases with three different microphysics schemes (REF: WSM 6;
746 MP2: Goddard; MP3: Thompson). The sensitivity of WRF simulated rain field to
747 microphysics parameterization illustrates the difficulty in reproducing the spatial and
748 temporal precipitation patterns as also concluded in previous studies (e.g. (Li et al., 2013)).
749 The results demonstrated that the total daily deposition is very sensitive to the microphysics
750 scheme and the WSM 6 microphysical scheme performed the best among the three schemes.

751 (2) The simulated total daily depositions generally agreed with the pattern observed in the
752 measurements. But the model did not estimate the observed deposition peaks and magnitudes
753 very well for both ^{131}I and ^{137}Cs . Wet deposition dominated over dry deposition at most of the
754 observation stations, but not at all locations in the simulated domain. Moreover, the dry and
755 wet depositions of different radionuclides are affected by wind and rainfall in different ways.
756 Based on SR, the resistance model and the simple parameterization for dry deposition yield
757 the best performance in capturing the total deposition of ^{131}I , while the model with constant
758 dry deposition velocity (0.05 cm s^{-1}) has the best performance in capturing the total
759 deposition of ^{137}Cs . Using the wet deposition parameterization based on precipitation rate can
760 better predict the total daily deposition of ^{131}I , while using the wet deposition

761 parameterizations based on relative humidity can better predict the total daily deposition of
762 ^{137}Cs . Again these finding could be related to differences between gaseous and particulate
763 species.

764 (3) The results illustrate that the total daily deposition is quite sensitive to the emission rate,
765 whose estimates by two different studies had large discrepancies. At some of the stations, the
766 gas partitioning of ^{131}I is also an important parameters that controls the total daily deposition.
767 The total deposition of ^{137}Cs is not very sensitive to the size distribution. Based on SR, case
768 REF (with emission estimated from JAEA) reproduced the observations more accurately than
769 case EM2 (with emission estimated from TEPCO); the cases with gaseous fractions of 30% or
770 60% had comparable performances and can better reproduce the total deposition of ^{131}I for
771 this particular event. The case with a log-normal distribution for the size of ^{137}Cs in the
772 emission has only a slightly better performance than the case with uniform particle size of
773 ^{137}Cs . Based on the averaged absolute value of the difference (AAD) between the error in the
774 reference case and that in different sensitivity cases, the total deposition is most sensitive to
775 the emission rate for both ^{131}I and ^{137}Cs , while it is not sensitive to the dry deposition
776 parameterizations since the dry deposition is just a minor fraction of the total deposition.
777 Moreover, based on AAD, for ^{131}I , the total daily deposition is moderately sensitive to the
778 microphysics schemes, the horizontal diffusion schemes, gas partitioning and wet deposition
779 parameterizations. For ^{137}Cs , the total daily deposition is also very sensitive to the
780 microphysics schemes and wet deposition parameterizations, and it is moderately sensitive to
781 the horizontal diffusion schemes and the size distribution.

782 (4) While the analysis allowed us to assess the important physics schemes and inputs that
783 significantly influenced model performance and to provide conclusions about what model
784 options and inputs seem to produce better outputs, general conclusions about the best model
785 configuration are difficult to make due the potential error cancelation between different
786 options and due to fact that for some cases the best configuration or input seem to vary from
787 one station to another. Despite this inherent uncertainty, it is clear that WRF/Chem is

788 generally able to produce realistic deposition patterns and values, and that temporal errors in
789 the deposition partially cancel out as evidenced by the lower values of the PBIAS compared
790 to PRMSE. Moreover, in many cases, simulations with different options bracket the
791 observation. As such, while it seems the uncertainty in inputs and configuration precludes
792 very high accuracy in simulations of ground deposition, ensemble simulations with different
793 options and a focus on accumulated deposition should prove useful in environmental impact
794 assessments for past or potential **future** accidents.

795 Finally, the current study has some limitations that the reader needs to bear in mind when
796 using the findings in other studies. First, changes during the transport and deposition
797 processes of the proportion of organic and inorganic forms **and of** the gas partitioning and the
798 particle size distributions were not considered in this study due to the limited knowledge of
799 these processes, though they may strongly affect the transport and deposition of radionuclides.
800 Second, a longer term assessment of the fate and transport of ^{137}Cs is not conducted in this
801 study, but it may be required for assessing the health and ecological impacts of the
802 radionuclides release since ^{137}Cs has a **very long half-life (~ 30 years)**. Future work involving
803 idealized cases to examine in more detail how weather conditions affect the atmospheric
804 transport and ground deposition of radionuclides is needed since our results confirm that
805 slight modifications in the wind fields and precipitation can significantly influence deposition.

806

807 **Acknowledgment**

808 This work was supported by the Ministry of Science and Technology of the People's Republic
809 of China under 863 (Grant No. 2012AA050907), the National Nature Science Foundation of
810 China (Grant No. 71373140), the State Key Laboratory of NBC Protection for Civilian
811 (No.SKLNBC0308), the Independent Research Program of Tsinghua University (2012Z10137)
812 and the Scientific Research Foundation for the Returned Overseas Chinese Scholars of the
813 State Education Ministry. EBZ and DL, and the one-year exchange visit of XH to Princeton
814 University, are partially supported by a grant from an anonymous donor aimed at studying

815 anthropogenic impacts on the hydrological cycle and water resources in China. We are
816 grateful to Maofeng Liu for helping us to process the figures and Ting Sun for providing the
817 forcing data used in the simulations.

818

819 **Appendix. The improvement to WRF/Chem**

820 In this paper, WRF/Chem is used to simulate the atmospheric transport and ground deposition
821 of radionuclides. The default WRF/Chem model has no radionuclides; to implement the
822 radionuclides into WRF/Chem, we add a new chemistry package to the registry file
823 *registry.chem* to include air concentration variables (in the *chem* array), ground deposition
824 variables (in the *misc* array) and variables related to the emissions (in the *emis_ant* array) of
825 ^{131}I and ^{137}Cs . Moreover, several modules in the *chem* subdirectory are modified to account
826 for new transport and deposition mechanisms. The radioactive decay process is added into the
827 advection-diffusion solver. Dry deposition parameterizations for gaseous species are added
828 into the *module_dep_simple*; while dry deposition parameterizations for particulate species
829 are added into the *module_gocart_drydep*. Wet deposition parameterizations are added into
830 the *module_wetscav_driver*. The emission rates used by the simulations are imported by the
831 program *prep_chem_sources*.

832

833 **References**

834 Andronopoulos, S., and Bartzis, J. G.: A gamma radiation dose calculation method for use
835 with Lagrangian puff atmospheric dispersion models used in real-time emergency response
836 systems, *J Radiol Prot*, 30, 747-759, Doi 10.1088/0952-4746/30/4/008, 2010.

837 Baklanov, A., and Sorensen, J. H.: Parameterisation of radionuclide deposition in atmospheric
838 long-range transport modelling, *Phys Chem Earth Pt B*, 26, 787-799, Doi
839 10.1016/S1464-1909(01)00087-9, 2001.

840 Basit, A., Espinosa, F., Avila, R., Raza, S., and Irfan, N.: Simulation of atmospheric dispersion

841 of radionuclides using an Eulerian-Lagrangian modelling system, *J Radiol Prot*, 28, 539-561,
842 Doi 10.1088/0952-4746/28/4/007, 2008.

843 Brandt, J., Christensen, J. H., and Frohn, L. M.: Modelling transport and deposition of
844 caesium and iodine from the Chernobyl accident using the DREAM model, *Atmos Chem*
845 *Phys*, 2, 397-417, 2002.

846 Chamberlain, A. C.: *Radioactive aerosols*, Cambridge environmental chemistry series, 3,
847 Cambridge University Press, Cambridge England ; New York, xii, 255 p. pp., 1991.

848 Chino, M., Nakayama, H., Nagai, H., Terada, H., Katata, G., and Yamazawa, H.: Preliminary
849 Estimation of Release Amounts of I-131 and Cs-137 Accidentally Discharged from the
850 Fukushima Daiichi Nuclear Power Plant into the Atmosphere, *J Nucl Sci Technol*, 48,
851 1129-1134, 2011.

852 Clark, M. J., and Smith, F. B.: Wet and Dry Deposition of Chernobyl Releases, *Nature*, 332,
853 245-249, Doi 10.1038/332245a0, 1988.

854 de Sampaio, P. A. B., Junior, M. A. G., and Lapa, C. M. F.: A CFD approach to the
855 atmospheric dispersion of radionuclides in the vicinity of NPPs, *Nucl Eng Des*, 238, 250-273,
856 DOI 10.1016/j.nucengdes.2007.05.009, 2008.

857 Grell, G. A., Peckham, S. E., Schmitz, R., McKeen, S. A., Frost, G., Skamarock, W. C., and
858 Eder, B.: Fully coupled "online" chemistry within the WRF model, *Atmos Environ*, 39,
859 6957-6975, DOI 10.1016/j.atmosenv.2005.04.027, 2005.

860 Huh, C. A., Hsu, S. C., and Lin, C. Y.: Fukushima-derived fission nuclides monitored around
861 Taiwan: Free tropospheric versus boundary layer transport, *Earth Planet Sc Lett*, 319, 9-14,
862 DOI 10.1016/j.epsl.2011.12.004, 2012.

863 Huh, C. A., Lin, C. Y., and Hsu, S. C.: Regional Dispersal of Fukushima-Derived Fission
864 Nuclides by East-Asian Monsoon: A Synthesis and Review, *Aerosol Air Qual Res*, 13,
865 537-544, DOI 10.4209/aaqr.2012.08.0223, 2013.

866 IAEA: Generic models for use in assessing the impact of discharges of radioactive substances

867 to the environment. International atomic energy agency, Vienna, 2001.

868 Jylha, K.: Empirical Scavenging Coefficients of Radioactive Substances Released from
869 Chernobyl, *Atmos Environ a-Gen*, 25, 263-270, Doi 10.1016/0960-1686(91)90297-K, 1991.

870 Kaneyasu, N., Ohashi, H., Suzuki, F., Okuda, T., and Ikemori, F.: Sulfate Aerosol as a
871 Potential Transport Medium of Radiocesium from the Fukushima Nuclear Accident, *Environ*
872 *Sci Technol*, 46, 5720-5726, Doi 10.1021/Es204667h, 2012.

873 Katata, G., Ota, M., Terada, H., Chino, M., and Nagai, H.: Atmospheric discharge and
874 dispersion of radionuclides during the Fukushima Dai-ichi Nuclear Power Plant accident. Part
875 I: Source term estimation and local-scale atmospheric dispersion in early phase of the
876 accident, *J Environ Radioactiv*, 109, 103-113, DOI 10.1016/j.jenvrad.2012.02.006, 2012.

877 Korsakissok, I., Mathieu, A., and Didier, D.: Atmospheric dispersion and ground deposition
878 induced by the Fukushima Nuclear Power Plant accident: A local-scale simulation and
879 sensitivity study, *Atmos Environ*, 70, 267-279, DOI 10.1016/j.atmosenv.2013.01.002, 2013.

880 Lauritzen, B., Baklanov, A., Mahura, A., Mikkelsen, T., and Sorensen, J. H.: Probabilistic risk
881 assessment for long-range atmospheric transport of radionuclides, *J Environ Radioactiv*, 96,
882 110-115, DOI 10.1016/j.jenvrad.2007.01.026, 2007.

883 Leelossy, A., Meszaros, R., and Lagzi, I.: Short and long term dispersion patterns of
884 radionuclides in the atmosphere around the Fukushima Nuclear Power Plant, *J Environ*
885 *Radioactiv*, 102, 1117-1121, DOI 10.1016/j.jenvrad.2011.07.010, 2011.

886 Li, D., Bou-Zeid, E., Baeck, M. L., Jessup, S., and Smith, J. A.: Modeling land surface
887 processes and heavy rainfall in urban environments: sensitivity to urban surface
888 representations, *J Hydrometeorol*, 14, 1098-1118, 10.1175/JHM-D-12-0154.1, 2013.

889 Lutman, E. R., Jones, S. R., Hill, R. A., McDonald, P., and Lambers, B.: Comparison between
890 the predictions of a Gaussian plume model and a Lagrangian particle dispersion model for
891 annual average calculations of long-range dispersion of radionuclides, *J Environ Radioactiv*,
892 75, 339-355, DOI 10.1016/j.jenvrad.2003.11.013, 2004.

893 Maryon, R. H., Smith, F. B., Conway, B. J., and Goddard, D. M.: The Uk Nuclear Accident
894 Model, *Prog Nucl Energ*, 26, 85-104, Doi 10.1016/0149-1970(91)90043-O, 1991.

895 **Masson, O. e. a.: Tracking of Airborne Radionuclides from the Damaged Fukushima Dai-Ichi**
896 **Nuclear Reactors by European Networks, *Environ Sci Technol*, 45, 7670-7677, Doi**
897 **10.1021/Es2017158, 2011.**

898 Mathieu, A., Korsakissok, I., Quelo, D., Groell, J., Tombette, M., Didler, D., Quentric, E.,
899 Saunier, O., Benoit, J. P., and Isnard, O.: Atmospheric Dispersion and Deposition of
900 Radionuclides from the Fukushima Daiichi Nuclear Power Plant Accident, *Elements*, 8,
901 195-200, DOI 10.2113/gselements.8.3.195, 2012.

902 **Momoshima, N., Sugihara, S., Ichikawa, R., and Yokoyama, H.: Atmospheric radionuclides**
903 **transported to Fukuoka, Japan remote from the Fukushima Dai-ichi nuclear power complex**
904 **following the nuclear accident, *J Environ Radioactiv*, 111, 28-32, DOI**
905 **10.1016/j.jenvrad.2011.09.001, 2012.**

906 Morino, Y., Ohara, T., and Nishizawa, M.: Atmospheric behavior, deposition, and budget of
907 radioactive materials from the Fukushima Daiichi nuclear power plant in March 2011,
908 *Geophys Res Lett*, 38, L00g11, Doi 10.1029/2011gl048689, 2011.

909 Morino, Y., Ohara, T., Watanabe, M., Hayashi, S., and Nishizawa, M.: Episode Analysis of
910 Deposition of Radiocesium from the Fukushima Daiichi Nuclear Power Plant Accident,
911 *Environ Sci Technol*, 47, 2314-2322, Doi 10.1021/Es304620x, 2013.

912 Pudykiewicz, J.: Simulation of the Chernobyl dispersion with a 3-D hemispheric tracer model,
913 *Tellus B*, 41, 391-412, DOI 10.1111/j.1600-0889.1989.tb00317.x, 1989.

914 Ristovski, Z. D. F., C.; D'Anna, B.; Johnson, G. R.; Bostrom, J. T.: Characterization of iodine
915 particles with Volatilization-Humidification Tandem Differential Mobility Analyser
916 (VH-TDMA), Raman and SEM techniques, *Atmospheric Chemistry and Physics Discussions*,
917 6 1481-1508, 2006.

918 Seinfeld, J. H., and Pandis, S. N.: Atmospheric chemistry and physics : from air pollution to

919 climate change, 2nd ed., J. Wiley, Hoboken, N.J., xxviii, 1203 p. pp., 2006.

920 Sportisse, B.: A review of parameterizations for modelling dry deposition and scavenging of
921 radionuclides, *Atmos Environ*, 41, 2683-2698, DOI 10.1016/j.atmosenv.2006.11.057, 2007.

922 Srinivas, C. V., Venkatesan, R., Baskaran, R., Rajagopal, V., and Venkatraman, B.: Regional
923 scale atmospheric dispersion simulation of accidental releases of radionuclides from
924 Fukushima Dai-ichi reactor, *Atmos Environ*, 61, 66-84, DOI 10.1016/j.atmosenv.2012.06.082,
925 2012.

926 Stohl, A., Seibert, P., Wotawa, G., Arnold, D., Burkhardt, J. F., Eckhardt, S., Tapia, C., Vargas,
927 A., and Yasunari, T. J.: Xenon-133 and caesium-137 releases into the atmosphere from the
928 Fukushima Dai-ichi nuclear power plant: determination of the source term, atmospheric
929 dispersion, and deposition, *Atmos Chem Phys*, 12, 2313-2343, DOI
930 10.5194/acp-12-2313-2012, 2012.

931 Stull, R. B.: An introduction to boundary layer meteorology, Atmospheric sciences library,
932 Kluwer Academic Publishers, Dordrecht ; Boston, xii, 666 p. pp., 1988.

933 Takemura, T., Nakamura, H., Takigawa, M., Kondo, H., Satomura, T., Miyasaka, T., and
934 Nakajima, T.: A Numerical Simulation of Global Transport of Atmospheric Particles Emitted
935 from the Fukushima Daiichi Nuclear Power Plant, *Sola*, 7, 101-104, DOI
936 10.2151/sola.2011-026, 2011.

937 Talbot, C., Bou-Zeid, E., and Smith, J.: Nested Mesoscale Large-Eddy Simulations with WRF:
938 Performance in Real Test Cases, *J Hydrometeorol*, 13, 1421-1441, Doi
939 10.1175/Jhm-D-11-048.1, 2012.

940 Ten Hoeve, J. E., and Jacobson, M. Z.: Worldwide health effects of the Fukushima Daiichi
941 nuclear accident, *Energ Environ Sci*, 5, 8743-8757, Doi 10.1039/C2ee22019a, 2012.

942 **Tepco: Estimation of Radioactive Material Released to the Atmosphere during the Fukushima**
943 **Daiichi NPS Accident, available at:**
944 **http://www.tepco.co.jp/en/press/corp-com/release/betu12_e/images/120524e0205.pdf (last**

945 [access: 6 April 2013](#)), 2012.

946 Terada, H., and Chino, M.: Development of an Atmospheric Dispersion Model for Accidental
947 Discharge of Radionuclides with the Function of Simultaneous Prediction for Multiple
948 Domains and its Evaluation by Application to the Chernobyl Nuclear Accident, *J Nucl Sci*
949 *Technol*, 45, 920-931, Doi 10.3327/Jnst.45.920, 2008.

950 Terada, H., Katata, G., Chino, M., and Nagai, H.: Atmospheric discharge and dispersion of
951 radionuclides during the Fukushima Dai-ichi Nuclear Power Plant accident. Part II:
952 verification of the source term and analysis of regional-scale atmospheric dispersion, *J*
953 *Environ Radioactiv*, 112, 141-154, DOI 10.1016/j.jenvrad.2012.05.023, 2012.

954 Till, J. E., and Grogan, H. A.: Radiological risk assessment and environmental analysis,
955 Oxford University Press, Oxford ; New York, xxvi, 702 p. pp., 2008.

956 Weast, R. C.: CRC handbook of chemistry and physics, 1st Student ed., CRC Press, Boca
957 Raton, FL, 1988.

958 Wesely, M. L.: Parameterization of Surface Resistances to Gaseous Dry Deposition in
959 Regional-Scale Numerical-Models, *Atmos Environ*, 23, 1293-1304, Doi
960 10.1016/0004-6981(89)90153-4, 1989.

961 Yamauchi, M.: Secondary wind transport of radioactive materials after the Fukushima
962 accident, *Earth Planets Space*, 64, E1-E4, DOI 10.5047/eps.2012.01.002, 2012.

963 Yasunari, T. J., Stohl, A., Hayano, R. S., Burkhart, J. F., Eckhardt, S., and Yasunari, T.:
964 Cesium-137 deposition and contamination of Japanese soils due to the Fukushima nuclear
965 accident, *P Natl Acad Sci USA*, 108, 19530-19534, DOI 10.1073/pnas.1112058108, 2011.

966 Zakaib, G. D.: Radiation risks unknown, *Nature*, 471, 419-419, 2011.

967

968 Table 1. Description of WRF simulations. In the column for wet deposition, ‘precipitation’ is
 969 short for the parameterization based on precipitation and ‘RH’ is short for the
 970 parameterization based on relative humidity.

Simulations	Emissions	Microphysics	Horizontal diffusion scheme	Gaseous fraction of ^{131}I	Size distribution	Dry deposition	Wet deposition
REF	JAEA	WSM 6	Smagorinsky	80%	Constant size	Resistance	Precipitation
EM2	TEPCO	WSM 6	Smagorinsky	80%	Constant size	Resistance	Precipitation
MP2	JAEA	Goddard	Smagorinsky	80%	Constant size	Resistance	Precipitation
MP3	JAEA	Thompson	Smagorinsky	80%	Constant size	Resistance	Precipitation
DIF2	JAEA	WSM 6	1.5-order TKE	80%	Constant size	Resistance	Precipitation
GP2	JAEA	WSM 6	Smagorinsky	100%	Constant size	Resistance	Precipitation
GP3	JAEA	WSM 6	Smagorinsky	60%	Constant size	Resistance	Precipitation
GP4	JAEA	WSM 6	Smagorinsky	30%	Constant size	Resistance	Precipitation
GP5	JAEA	WSM 6	Smagorinsky	0%	Constant size	Resistance	Precipitation
SD2	JAEA	WSM 6	Smagorinsky	80%	Log-Normal	Resistance	Precipitation
DRY2	JAEA	WSM 6	Smagorinsky	80%	Constant size	Simple	Precipitation
DRY3	JAEA	WSM 6	Smagorinsky	80%	Constant size	Constant v_d	Precipitation
WET2	JAEA	WSM 6	Smagorinsky	80%	Constant size	Resistance	RH

1 Table 2. The PBIAS and PRMSE of wind speed and MBE of wind direction with different
 2 horizontal diffusion schemes. ‘YA’, ‘CH’, ‘TOK’, ‘ON’, ‘NI’, ‘MA’, ‘SE’ and ‘IS’ represent
 3 the stations ‘YAMAGATA’, ‘CHIBA’, ‘TOKYO’, ‘ONAHAMA’, ‘NIIGATA’, ‘MAEBASHI’,
 4 ‘SENDAI’ and ‘ISHINOMAKI’, respectively.

Errors	Cases	YA	CH	TOK	ON	NI	MA	SE	IS
PBIAS	of REF	124 %	4%	28%	16%	58%	57%	7%	4%
wind speed	DIF2	127%	2%	27%	19 %	57%	64%	11%	3%
PRMSE	of REF	170%	51%	73%	62%	76%	93%	65%	56%
wind speed	DIF2	176%	50%	73%	63%	76%	98%	64%	56.57%
MBE of wind	REF	49.2	28.4	32.7	34.3	24.9	37.0	43.1	30.3
direction	DIF2	50.0	30.9	31.4	33.6	23.5	36.2	42.2	26.7

1 Table 3. The PBIAS and PRMSE of precipitation with different microphysics schemes. ‘YA’,
 2 ‘CH’, ‘TOK’, ‘ON’, ‘NI’, ‘MA’, ‘SE’ and ‘IS’ represent the stations ‘YAMAGATA’, ‘CHIBA’,
 3 ‘TOKYO’, ‘ONAHAMA’, ‘NIIGATA’, ‘MAEBASHI’, ‘SENDAI’ and ‘ISHINOMAKI’,
 4 respectively.

Errors	Cases	YA	CH	TOK	ON	NI	MA	SE	IS
PBIAS	REF	-17%	2%	29%	18%	-20%	14%	-7%	285%
	MP2	5%	35%	30%	13%	-33%	50%	24%	489%
	MP3	-9%	3%	1%	18%	-33%	39%	28%	282%
PRMSE	REF	190%	101%	282%	136%	182%	197%	204%	463%
	MP2	156%	153%	297%	196%	177%	213%	198%	1009%
	MP3	157%	118%	250%	149%	172%	156%	215%	414%

1 Table 4. The PBIAS and PRMSE of total daily depositions of ^{131}I and ^{137}Cs with different
2 horizontal diffusion schemes. GR represents the global ranks for PBIAS or PRMSE, and SR
3 represents for the sum of the global ranks. ‘YA’, ‘IB’, ‘TOC’, ‘GU’, ‘SA’, ‘CH’ and ‘TOK’
4 represent the stations ‘YAMAGATA’, ‘IBARAKI’, ‘TOCHIGI’, ‘GUNMA’, ‘SAITAMA’,
5 ‘CHIBA’ and ‘TOKYO’, respectively.

Errors	Cases	YA	IB	TOC	GU	SA	CH	TOK	GR	SR
PBIAS	REF	-36%	-82%	-46%	-39%	-75%	-87%	-80%	12	24
of ^{131}I	DIF2	-28%	-80%	-55%	-55%	-72%	-84%	-79%	<u>9</u>	<u>18</u>
PRMSE	REF	235%	187%	149%	87%	151%	187%	176%	12	24
of ^{131}I	DIF2	288%	183%	143%	134%	150%	181%	174%	<u>9</u>	<u>18</u>
PBIAS	REF	-36%	-43%	218%	157%	65%	-34%	-5%	11	22
of ^{137}Cs	DIF2	-51%	-43%	203%	96%	80%	-29%	-1%	<u>9</u>	<u>19</u>
PRMSE	REF	55%	167%	977%	452%	369%	52%	44%	11	22
of ^{137}Cs	DIF2	97%	168%	972%	317%	416%	39%	51%	<u>10</u>	<u>19</u>

1 Table 5. The PBIAS and PRMSE of total daily depositions of ^{131}I and ^{137}Cs with different
 2 microphysics schemes. GR represents the global ranks for PBIAS or PRMSE, and SR
 3 represents for the sum of the global ranks. ‘YA’, ‘IB’, ‘TOC’, ‘GU’, ‘SA’, ‘CH’ and ‘TOK’
 4 represent the stations ‘YAMAGATA’, ‘IBARAKI’, ‘TOCHIGI’, ‘GUNMA’, ‘SAITAMA’,
 5 ‘CHIBA’ and ‘TOKYO’, respectively.

Errors	Cases	YA	IB	TOC	GU	SA	CH	TOK	GR	SR
PBIAS of ^{131}I	REF	-36%	-82%	-46%	-39%	-75%	-87%	-80%	<u>12</u>	<u>23</u>
	MP2	-22%	-87%	-66%	-8%	-71%	-90%	-84%	<u>12</u>	<u>24</u>
	MP3	-34%	-89%	-51%	23%	-83%	-94%	-85%	18	35
PRMSE of ^{131}I	REF	235%	187%	149%	87%	151%	187%	176%	<u>11</u>	<u>23</u>
	MP2	334%	194%	145%	79%	150%	192%	181%	<u>12</u>	<u>24</u>
	MP3	104%	200%	145%	173%	158%	201%	182%	17	35
PBIAS of ^{137}Cs	REF	-36%	-43%	218%	157%	65%	-34%	-5%	<u>10</u>	<u>20</u>
	MP2	-48%	-62%	192%	297%	83%	-42%	-26%	16	31
	MP3	8%	-55%	272%	496%	17%	-73%	-29%	16	33
PRMSE of ^{137}Cs	REF	55%	167%	977%	452%	369%	52%	44%	<u>10</u>	<u>20</u>
	MP2	90%	169%	926%	763%	431%	78%	48%	15	31
	MP3	154%	142%	1216%	1207%	227%	176%	50%	17	33

1 Table 6. The PBIAS and PRMSE of total daily depositions of ^{131}I and ^{137}Cs with different dry
2 deposition schemes. GR represents the global ranks for PBIAS or PRMSE, and SR represents
3 for the sum of the global ranks. ‘YA’, ‘IB’, ‘TOC’, ‘GU’, ‘SA’, ‘CH’ and ‘TOK’ represent the
4 stations ‘YAMAGATA’, ‘IBARAKI’, ‘TOCHIGI’, ‘GUNMA’, ‘SAITAMA’, ‘CHIBA’ and
5 ‘TOKYO’, respectively.

Errors	Cases	YA	IB	TOC	GU	SA	CH	TOK	GR	SR
PBIAS of ^{131}I	REF	-36%	-82%	-46%	-39%	-75%	-87%	-80%	<u>7</u>	<u>16</u>
	DRY2	-36%	-82%	-46%	-39%	-75%	-87%	-80%	<u>7</u>	<u>16</u>
	DRY3	-50%	-82%	-69%	-45%	-79%	-87%	-82%	17	28
PRMSE of ^{131}I	REF	235%	187%	149%	87%	151%	187%	176%	<u>9</u>	<u>16</u>
	DRY2	235%	187%	149%	87%	151%	187%	176%	<u>9</u>	<u>16</u>
	DRY3	257%	186%	148%	104%	155%	187%	179%	11	28
PBIAS of ^{137}Cs	REF	-36%	-43%	218%	157%	65%	-34%	-5%	11	26
	DRY2	-36%	-43%	217%	157%	65%	-34%	-5%	<u>10</u>	22
	DRY3	-39%	-44%	212%	153%	59%	-35%	-7%	11	<u>20</u>
PRMSE of ^{137}Cs	REF	55%	167%	977%	452%	369%	52%	44%	15	26
	DRY2	55%	167%	974%	451%	368%	52%	44%	12	22
	DRY3	59%	166%	963%	442%	353%	55%	40%	<u>9</u>	<u>20</u>

1 Table 7. The PBIAS and PRMSE of total daily depositions of ^{131}I and ^{137}Cs with different wet
 2 deposition schemes. GR represents the global ranks for PBIAS or PRMSE, and SR represents
 3 for the sum of the global ranks. ‘YA’, ‘IB’, ‘TOC’, ‘GU’, ‘SA’, ‘CH’ and ‘TOK’ represent the
 4 stations ‘YAMAGATA’, ‘IBARAKI’, ‘TOCHIGI’, ‘GUNMA’, ‘SAITAMA’, ‘CHIBA’ and
 5 ‘TOKYO’, respectively.

Errors	Cases	YA	IB	TOC	GU	SA	CH	TOK	GR	SR
PBIAS	REF	-36%	-82%	-46%	-39%	-75%	-87%	-80%	<u>8</u>	<u>17</u>
of ^{131}I	WET2	-25%	-89%	-64%	-57%	-75%	-91%	-82%	12	24
PRMSE	REF	235%	187%	149%	87%	151%	187%	176%	<u>9</u>	<u>17</u>
of ^{131}I	WET2	219%	198%	144%	154%	152%	195%	178%	12	24
PBIAS	REF	-36%	-43%	218%	157%	65%	-34%	-5%	12	22
of ^{137}Cs	WET2	-31%	-65%	64%	56%	87%	-30%	3%	<u>9</u>	<u>20</u>
PRMSE	REF	55%	167%	977%	452%	369%	52%	44%	<u>10</u>	22
of ^{137}Cs	WET2	61%	172%	445%	228%	414%	47%	56%	11	<u>20</u>

1 Table 8. The PBIAS and PRMSE of total daily depositions of ^{131}I and ^{137}Cs with different
 2 emission rates. GR represents the global ranks for PBIAS or PRMSE, and SR represents for
 3 the sum of the global ranks. ‘YA’, ‘IB’, ‘TOC’, ‘GU’, ‘SA’, ‘CH’ and ‘TOK’ represent the
 4 stations ‘YAMAGATA’, ‘IBARAKI’, ‘TOCHIGI’, ‘GUNMA’, ‘SAITAMA’, ‘CHIBA’ and
 5 ‘TOKYO’, respectively.

Errors	Cases	YA	IB	TOC	GU	SA	CH	TOK	GR	SR
PBIAS	REF	-36%	-82%	-46%	-39%	-75%	-87%	-80%	<u>10</u>	<u>18</u>
of ^{131}I	EM2	-61%	-100%	-38%	920%	45%	-87%	-9%	11	23
PRMSE	REF	235%	187%	149%	87%	151%	187%	176%	<u>8</u>	<u>18</u>
of ^{131}I	EM2	199%	223%	161%	3395%	434%	187%	253%	12	23
PBIAS	REF	-36%	-43%	218%	157%	65%	-34%	-5%	<u>8</u>	<u>15</u>
of ^{137}Cs	EM2	-65%	-81%	204%	775%	128%	-47%	15%	13	27
PRMSE	REF	55%	167%	977%	452%	369%	52%	44%	<u>7</u>	<u>15</u>
of ^{137}Cs	EM2	148%	192%	1003%	1831%	595%	85%	115%	14	27

1 Table 9. The PBIAS and PRMSE of total daily depositions of ^{131}I with different gas
 2 partitioning of ^{131}I . GR represents the global ranks for PBIAS or PRMSE, and SR represents
 3 for the sum of the global ranks. ‘YA’, ‘IB’, ‘TOC’, ‘GU’, ‘SA’, ‘CH’ and ‘TOK’ represent the
 4 stations ‘YAMAGATA’, ‘IBARAKI’, ‘TOCHIGI’, ‘GUNMA’, ‘SAITAMA’, ‘CHIBA’ and
 5 ‘TOKYO’, respectively.

Errors	Cases	YA	IB	TOC	GU	SA	CH	TOK	GR	SR
PBIAS of ^{131}I	REF	-36%	-82%	-46%	-39%	-75%	-87%	-80%	22	39
	GP2	-47%	-93%	-45%	-60%	-86%	-96%	-93%	29	52
	GP3	-25%	-72%	-44%	-18%	-63%	-78%	-68%	14	<u>27</u>
	GP4	7%	-56%	-41%	14%	-44%	-62%	-51%	<u>7</u>	28
	GP5	-63%	-91%	-79%	-69%	-90%	-95%	-93%	33	63
PRMSE of ^{131}I	REF	235%	187%	149%	87%	151%	187%	176%	17	39
	GP2	233%	207%	136%	152%	164%	206%	197%	23	52
	GP3	240%	173%	152%	63%	150%	172%	165%	<u>13</u>	<u>27</u>
	GP4	273%	167%	155%	144%	171%	158%	169%	21	28
	GP5	257%	203%	161%	181%	169%	204%	197%	30	63

1 Table 10. The PBIAS and PRMSE of total daily depositions of ^{137}Cs with different size
 2 distribution of ^{137}Cs . GR represents the global ranks for PBIAS or PRMSE, and SR represents
 3 for the sum of the global ranks. ‘YA’, ‘IB’, ‘TOC’, ‘GU’, ‘SA’, ‘CH’ and ‘TOK’ represent the
 4 stations ‘YAMAGATA’, ‘IBARAKI’, ‘TOCHIGI’, ‘GUNMA’, ‘SAITAMA’, ‘CHIBA’ and
 5 ‘TOKYO’, respectively.

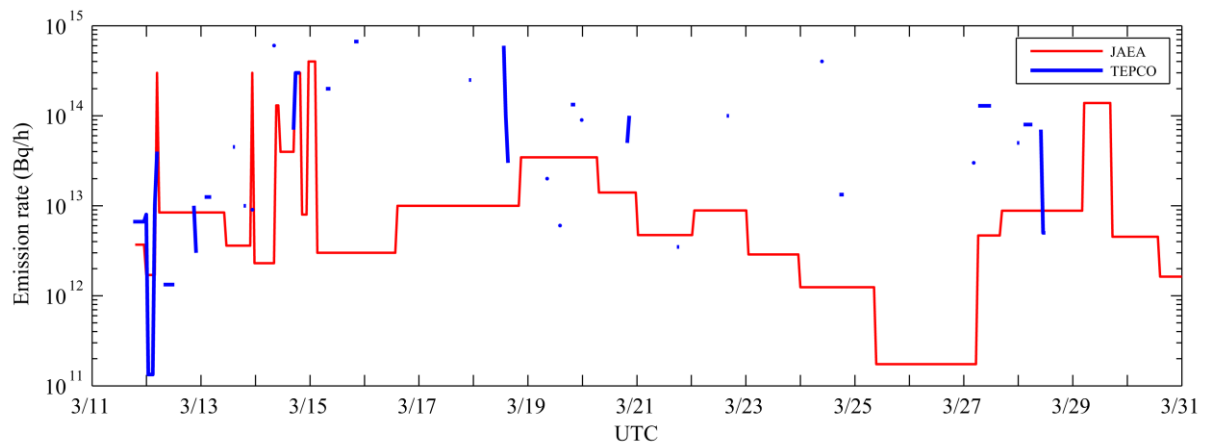
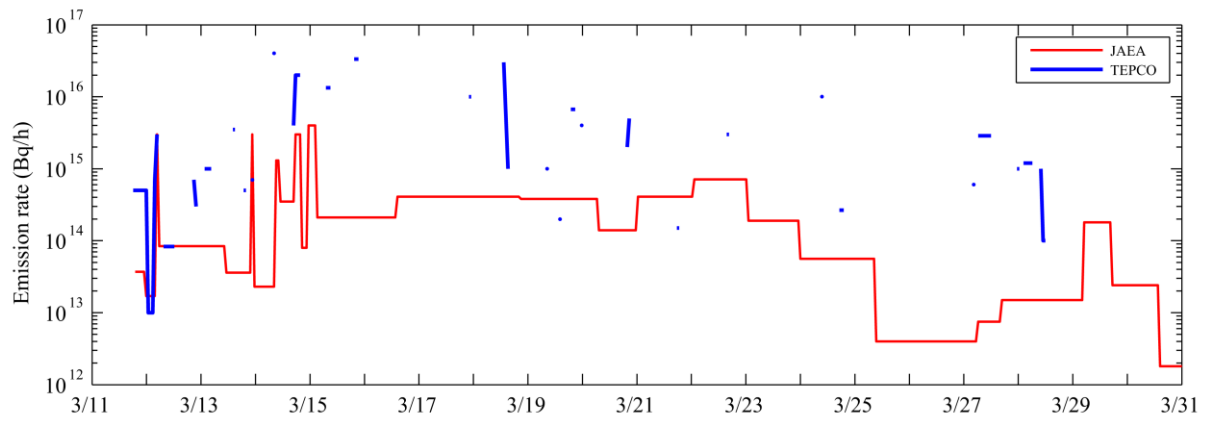
Errors	Cases	YA	IB	TOC	GU	SA	CH	TOK	GR	SR
PBIAS	REF	-36%	-43%	218%	157%	65%	-34%	-5%	12	22
of ^{137}Cs	SD2	-26%	-42%	212%	169%	88%	-18%	3%	<u>9</u>	<u>20</u>
PRMSE	REF	55%	167%	977%	452%	369%	52%	44%	<u>10</u>	22
of ^{137}Cs	SD2	45%	168%	963%	479%	430%	28%	56%	11	<u>20</u>

6

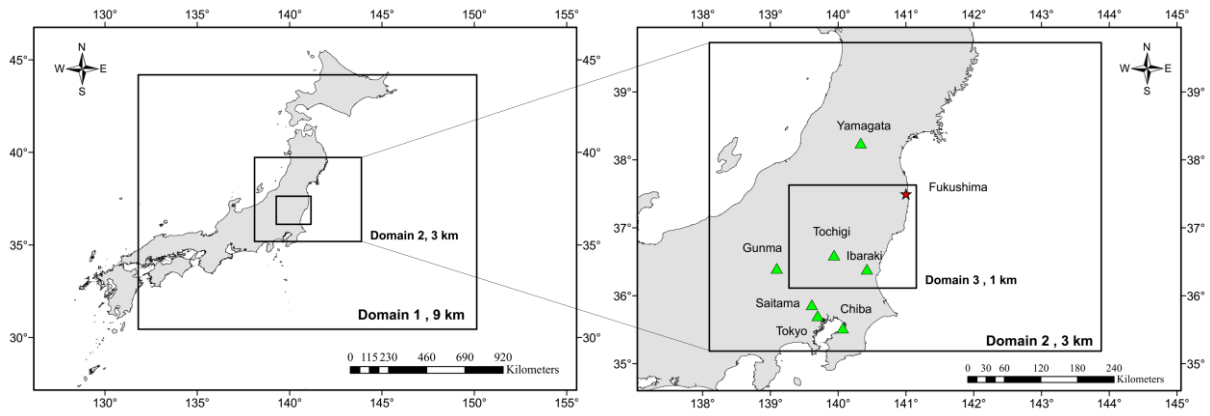
7

8 Table 11. The averaged absolute value of the difference (AAD) between the error in the
 9 reference case and that in different sensitivity cases.

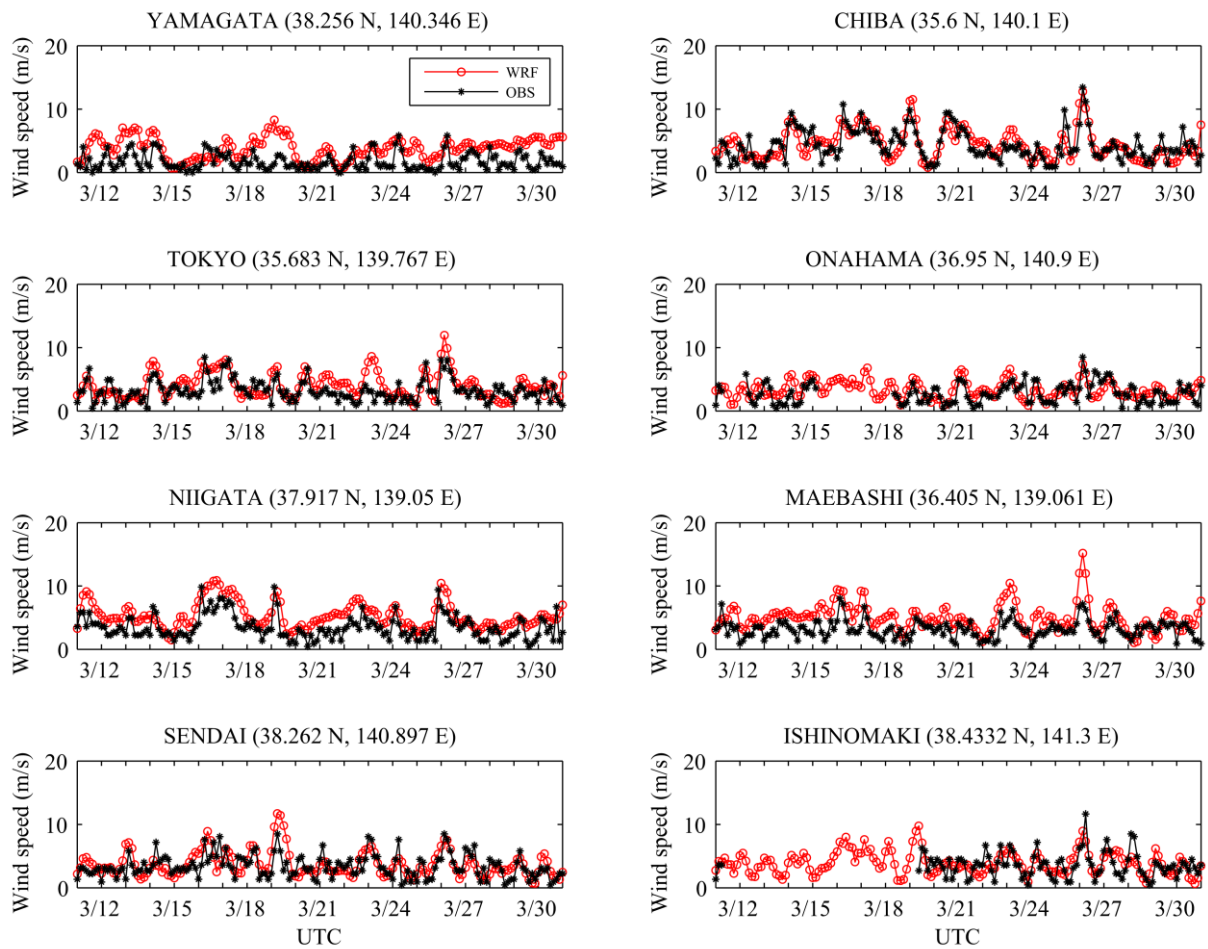
	AAD (PBIAS of ¹³¹ I)	AAD (PRMSE of ¹³¹ I)	AAD (PBIAS of ¹³⁷ Cs)	AAD (PRMSE of ¹³⁷ Cs)
REF - EM2	172%	536%	114%	265%
REF - MP2	11%	19%	35%	70%
REF - MP3	13%	37%	80%	199%
REF - DIF2	6%	17%	16%	36%
REF - GP2	11%	22%	-	-
REF - GP3	11%	10%	-	-
REF - GP4	30%	25%	-	-
REF - GP5	19%	28%	-	-
REF - SD2	-	-	11%	21%
REF - DRY2	0.02%	0.03%	0.20%	0.53%
REF - DRY3	7.17%	6.69%	3.46%	7.33%
REF - WET2	9%	16%	45%	118%



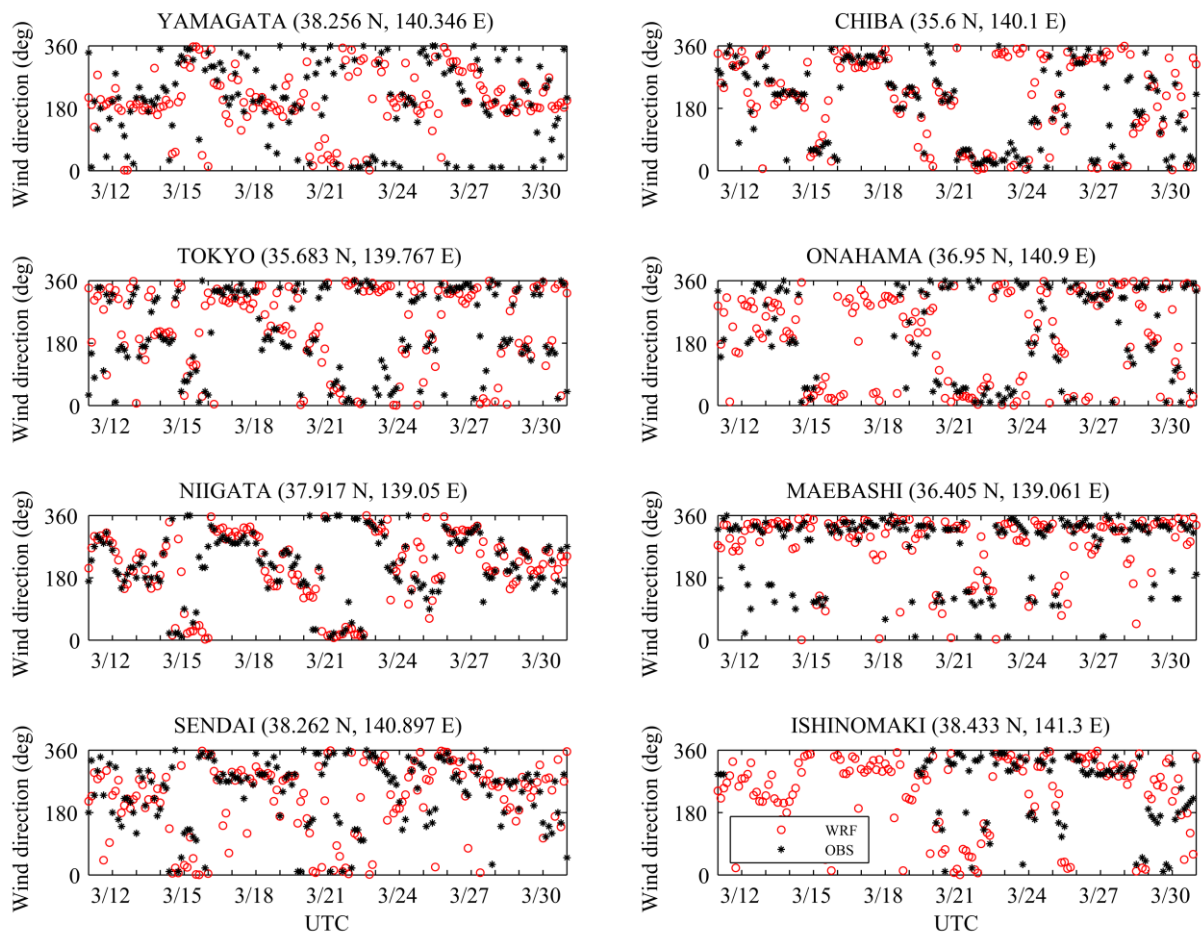
1
 2 Fig. 1. The estimated emission rates of ^{131}I and ^{137}Cs . Top panel: ^{131}I . Bottom panel: ^{137}Cs . The
 3 y-axis is the hourly radiological activity ($\text{Bq}\cdot\text{h}^{-1}$). The emission rate for TEPCO is calculated
 4 based on the release amount and duration provided by TEPCO.



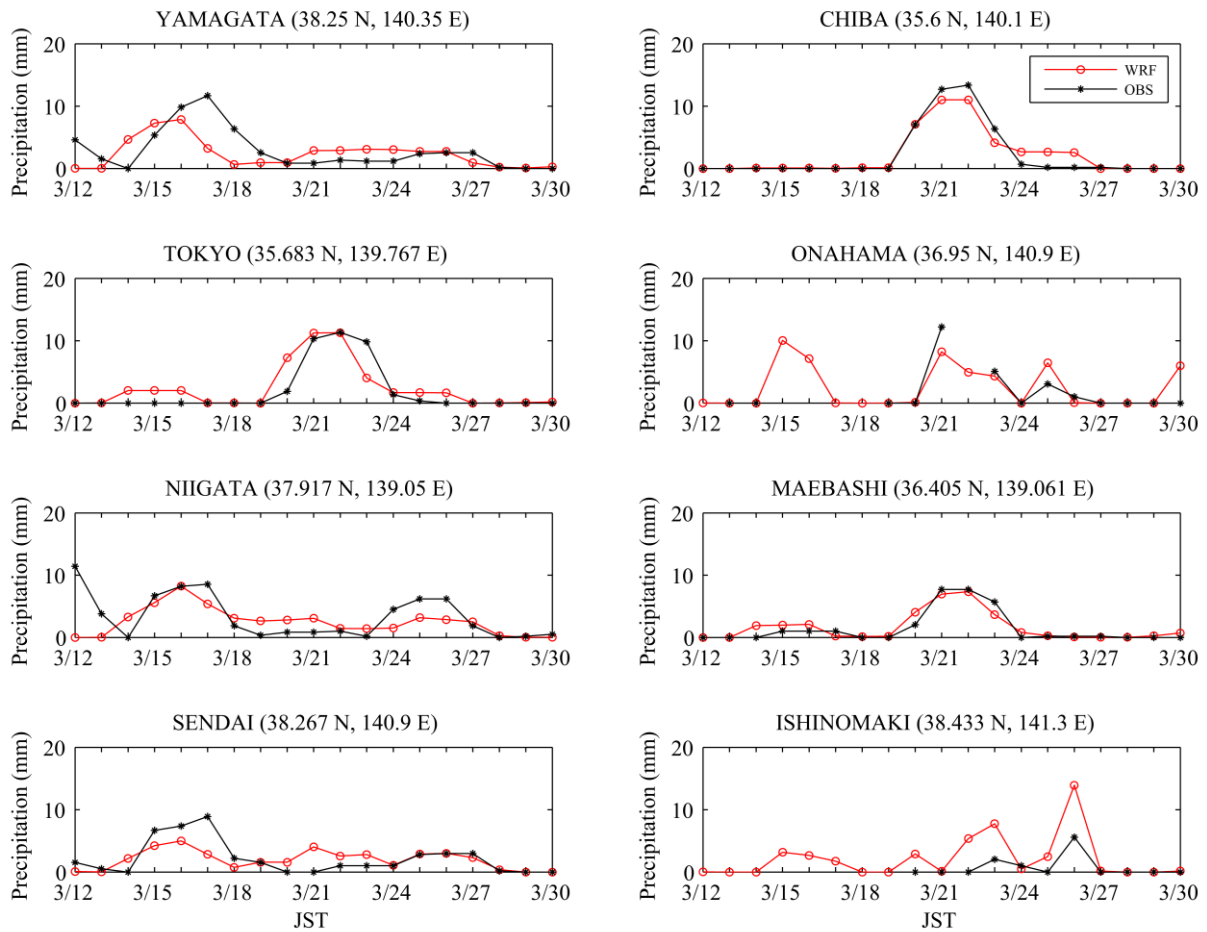
1
 2 Fig. 2. The WRF domain configurations and observational stations. Left: Domain 1, 2 and 3.
 3 Right: Domain 2 and 3. The red star on the right panel represents FNDPP (source of
 4 radioactive release) and the green triangles represent observational stations where deposition
 5 of radionuclides was measured (other stations are used for evaluation of the meteorological
 6 outputs of WRF).



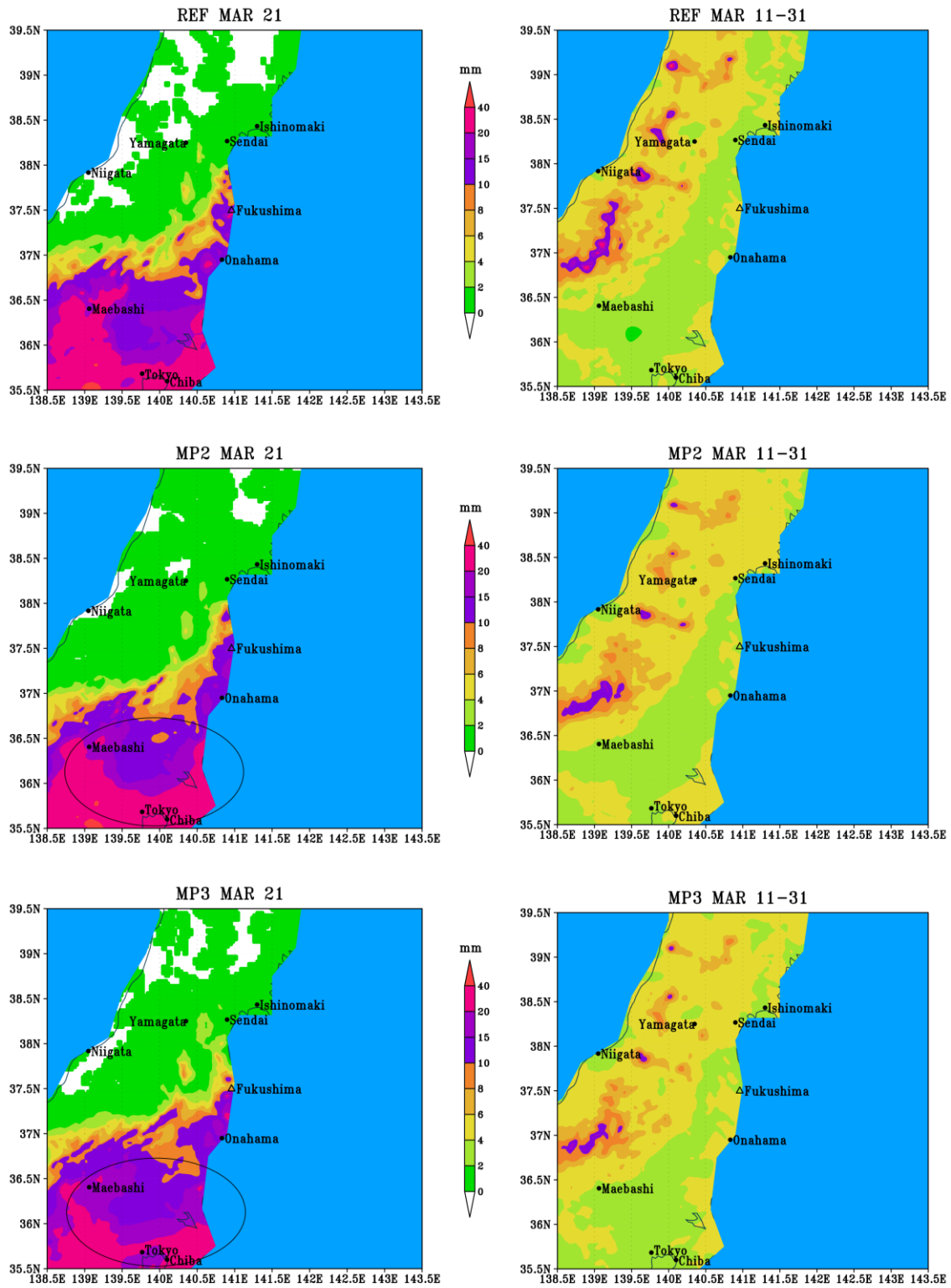
1
 2 Fig. 3. Simulated and observed surface wind speeds at 8 stations over Japan during the period
 3 from 00 UTC March 11 to 00 UTC March 31, 2011 (case REF). Output from the simulation is
 4 collected every 1 hour, but we only display on the figure data with 3-hour resolution for
 5 clarity. Red circles represent the simulated data from WRF and the black asterisks represent
 6 the observed data.



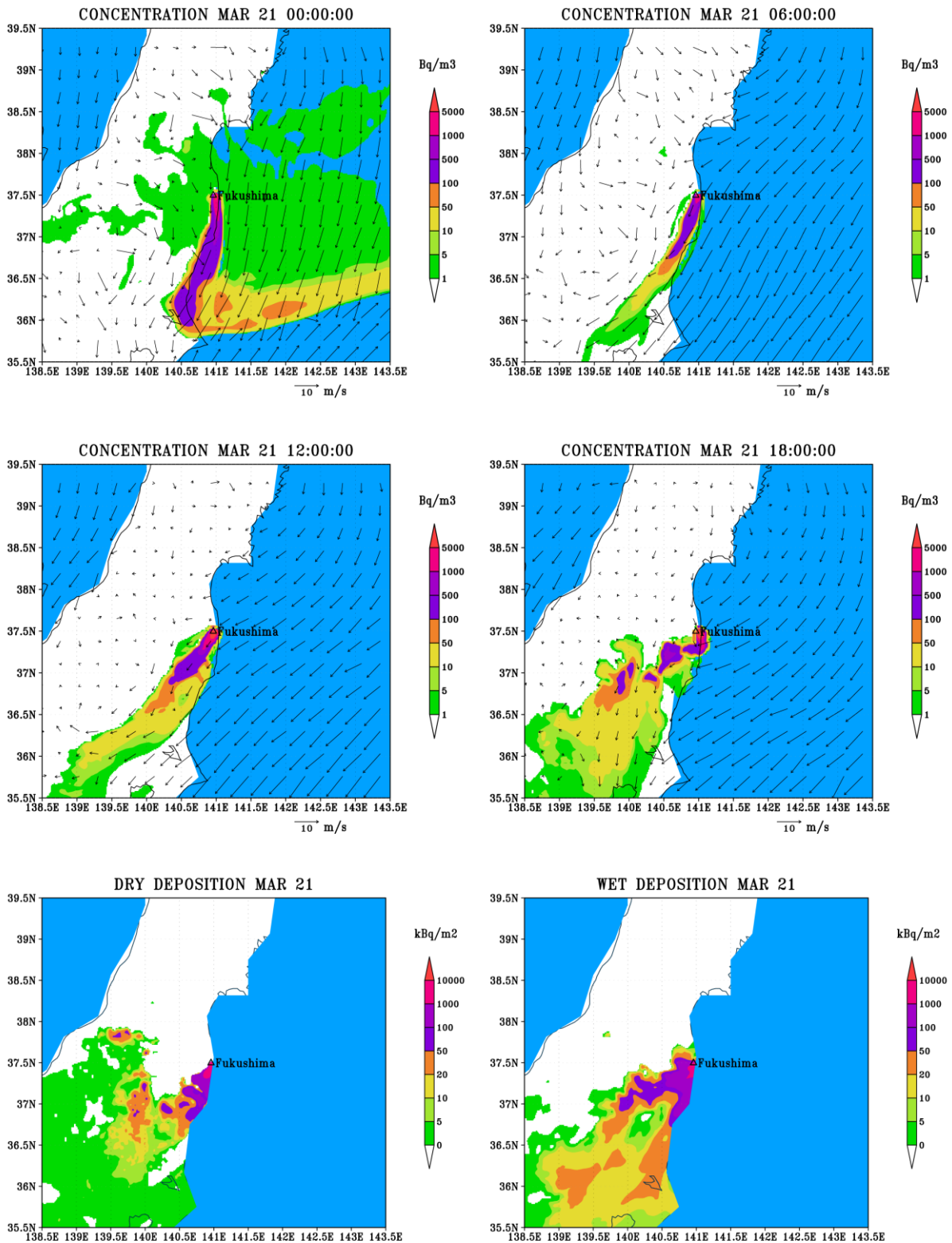
1
 2 Fig. 4. Simulated and observed surface wind directions at 8 stations over Japan during the
 3 period from 00 UTC March 11 to 00 UTC March 31, 2011 (case REF). Output from the
 4 simulation is collected every 1 hour, but we only display on the figure data with 3-hour
 5 resolution for clarity. Red circles represent the simulated data from WRF and the black
 6 asterisks represent the observed data.



1
 2 Fig. 5. Simulated and observed daily precipitation at 8 stations over Japan during the period
 3 from Japan Standard Time (JST = UTC + 9) March 11 to 31 2011. Red circles represent the
 4 simulated data from WRF and the black asterisks represent the observed data.

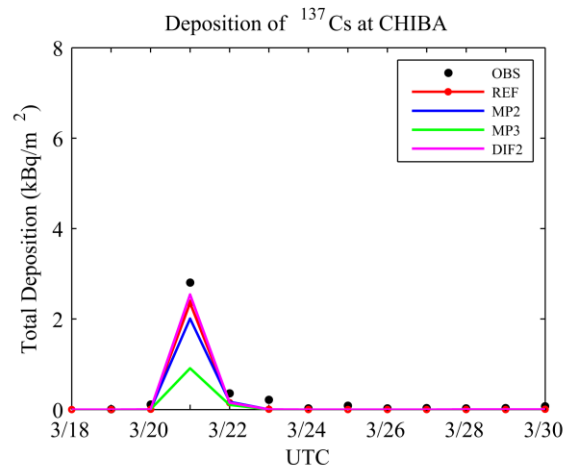
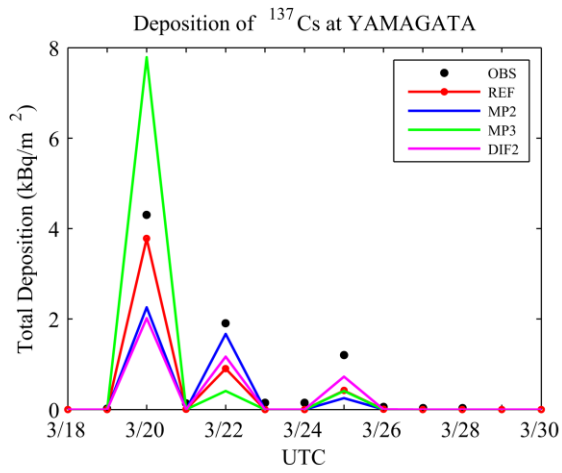
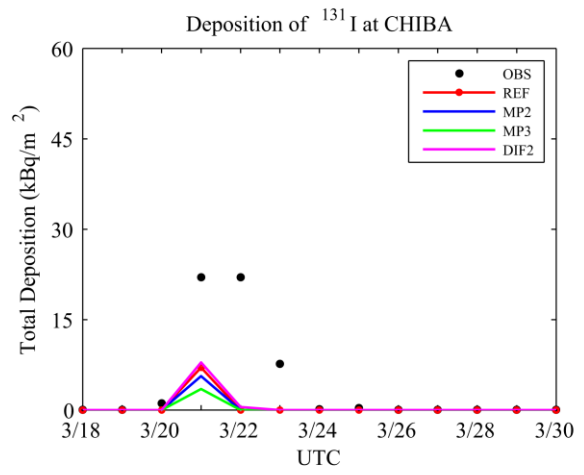
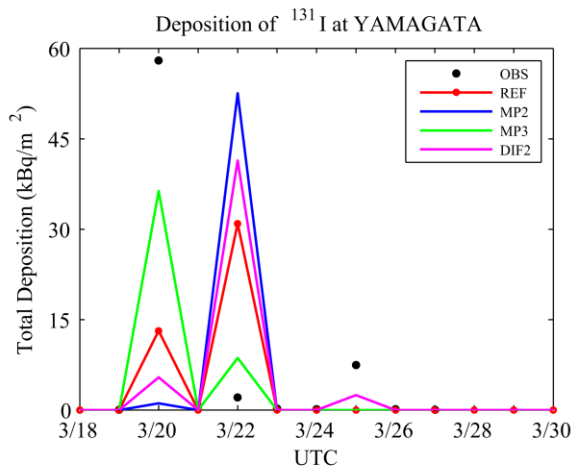


1
 2 Fig. 6. The simulated precipitation over domain 2 with 3 different microphysics schemes.
 3 Microphysics schemes WSM 6, Goddard and Thompson are used in case REF, MP2 and MP3,
 4 respectively. The left column shows the daily precipitation on March 21 and the right column
 5 shows the accumulated precipitation from March 11 to 31.

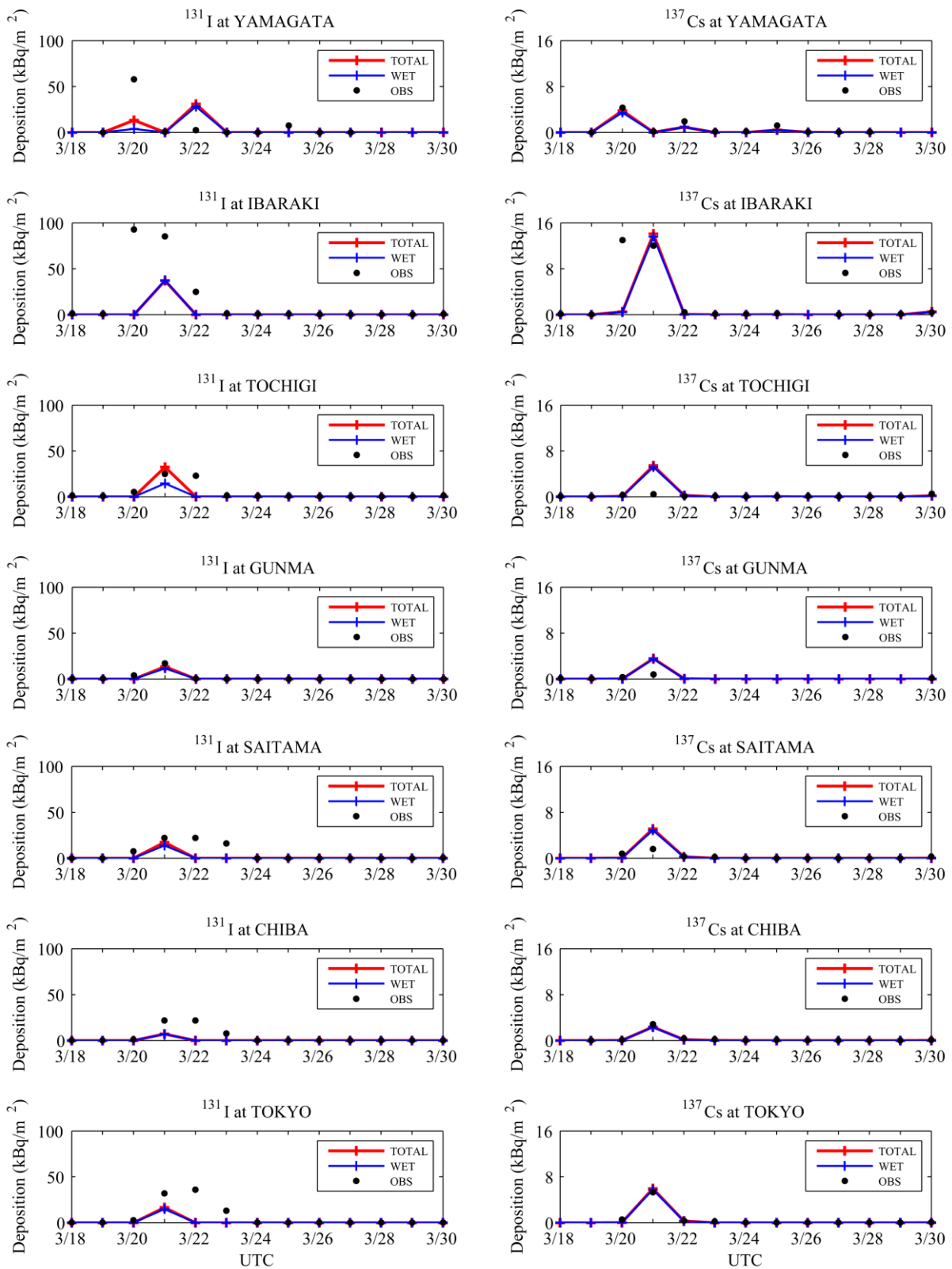


1
 2 Fig. 7. The near-surface concentration and ground deposition of ¹³¹I on March 21. The upper
 3 four panels show the distribution of concentration of ¹³¹I at the lowest level of the
 4 atmospheric model at four different times (i.e., 00, 06, 12, 18 UTC) on March 21, in which

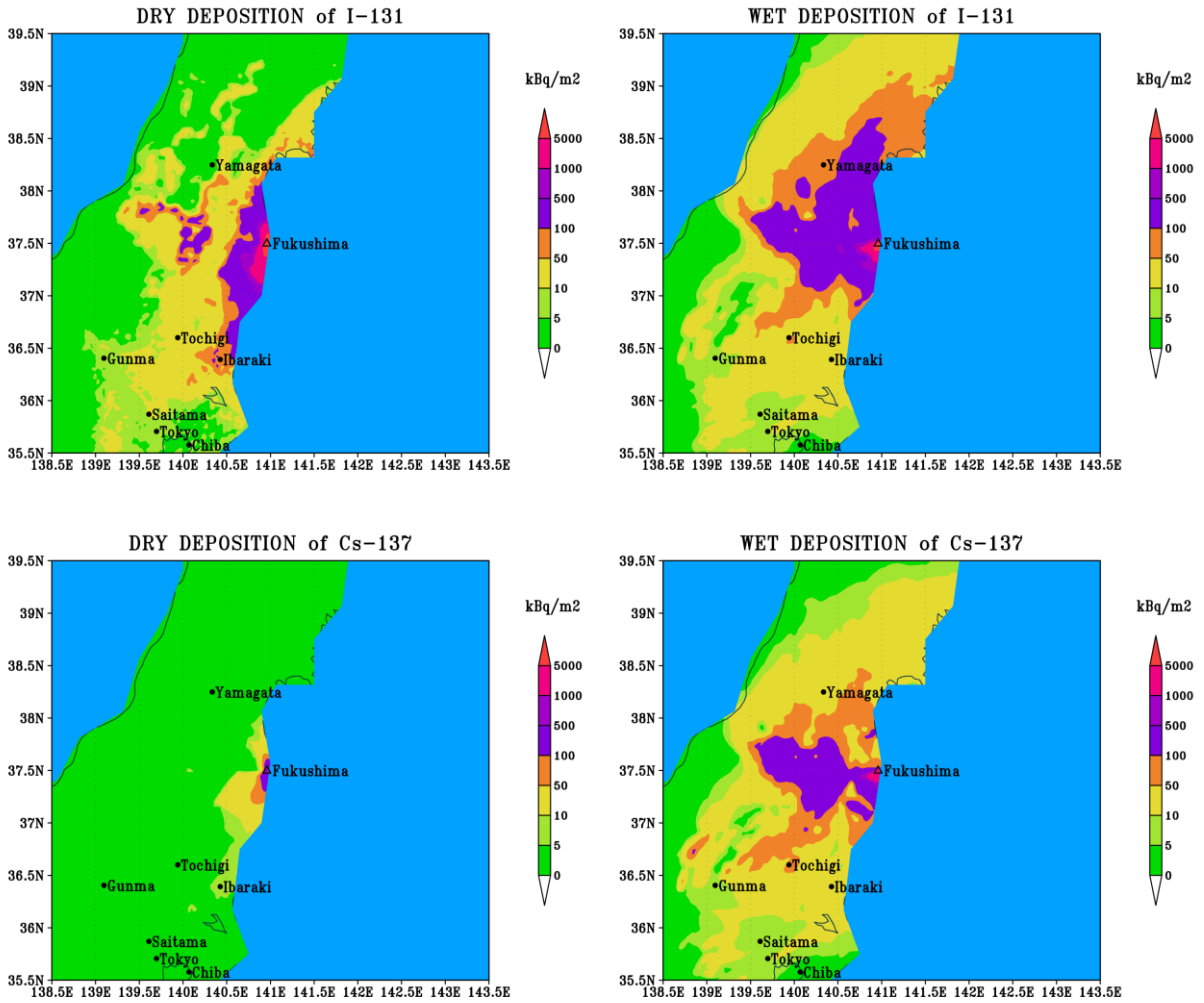
5 the near-surface concentration is represented by instantaneous values. The bottom panels
6 show the dry and wet deposition accumulated during March 21. The results are from the
7 simulation REF.



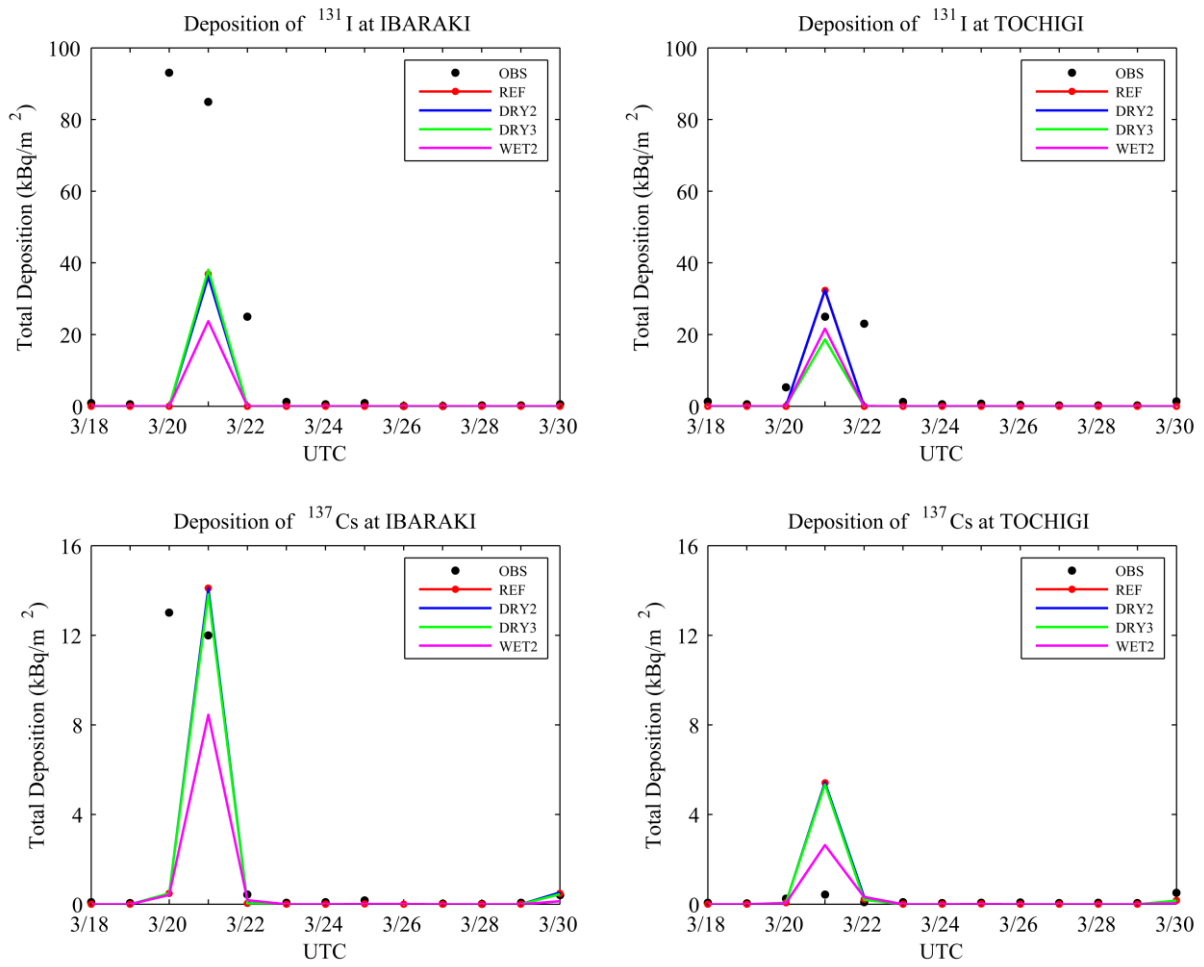
1
 2 Fig. 8. Daily total depositions in station YAMAGATA and CHIBA with different horizontal
 3 diffusion and microphysics schemes.



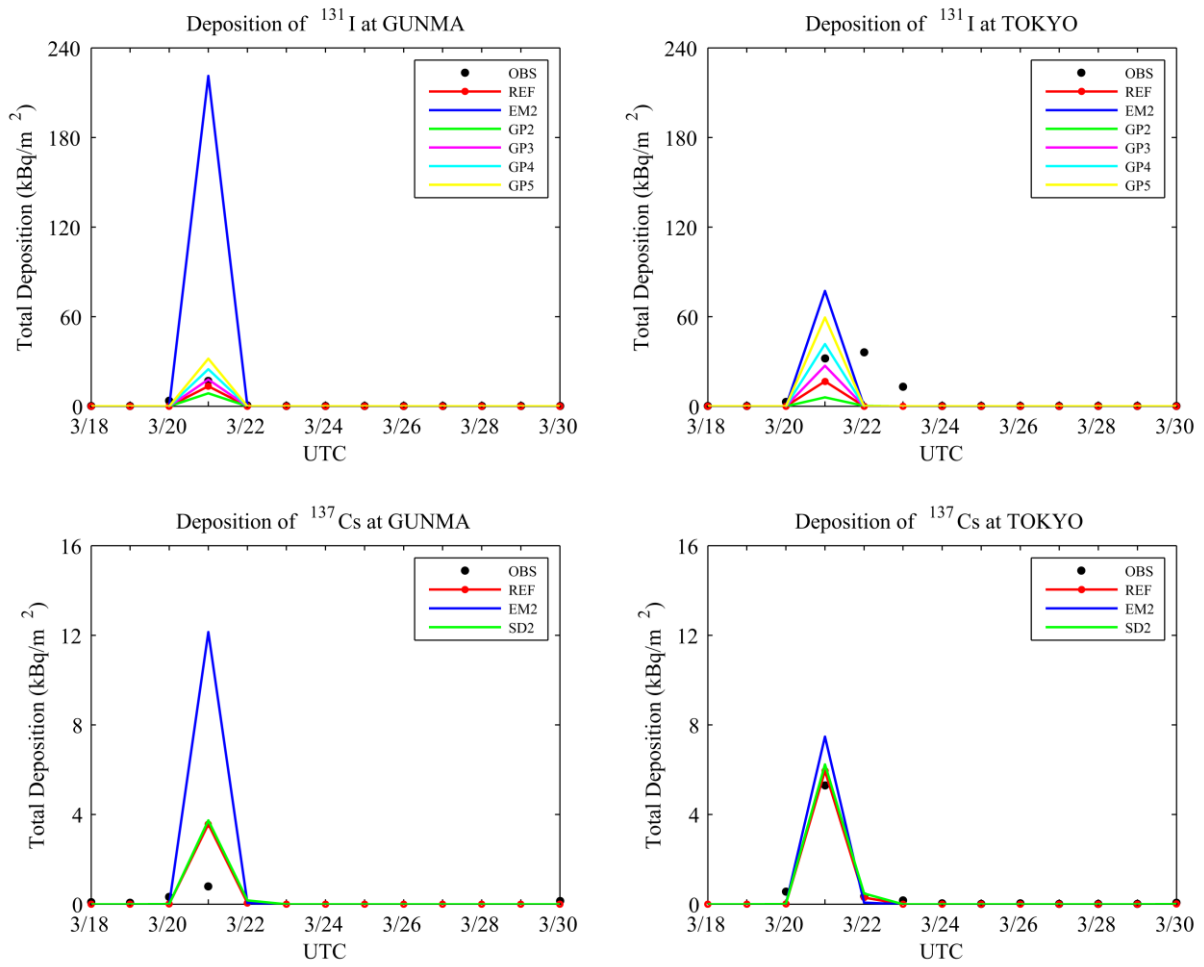
1
 2 Fig. 9. The comparison between simulated (REF case) total daily depositions and the
 3 observed data of ^{131}I and ^{137}Cs .



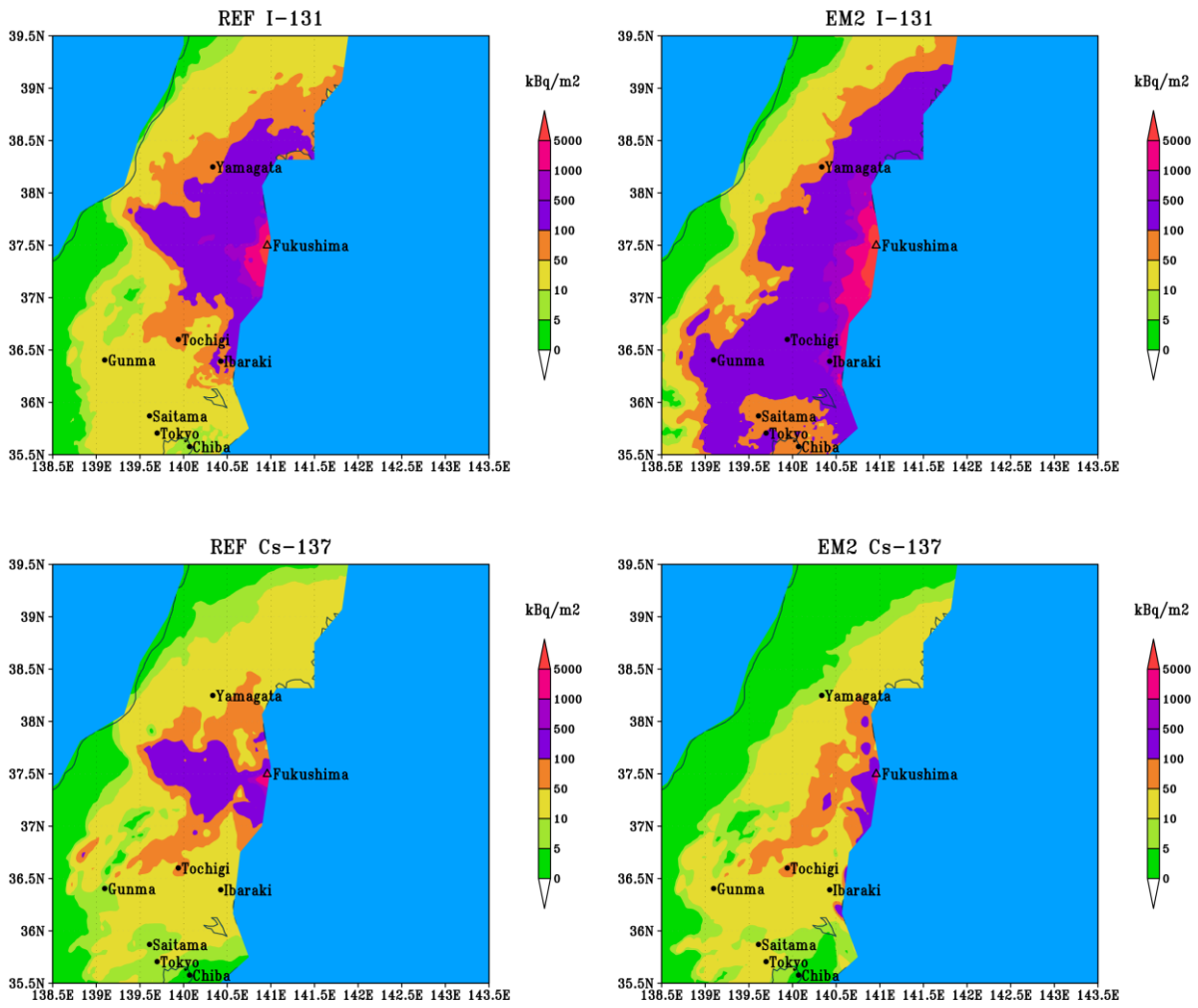
1
 2 Fig. 10. Distribution of accumulated dry and wet depositions of ^{131}I and ^{137}Cs over domain 2
 3 in the reference case (REF) from March 11 to March 31. The upper panels show the
 4 accumulated dry and wet deposition of ^{131}I ; the area with dry deposition over 100 kBq/m² is
 5 concentrated near the source and is much smaller than the area with wet deposition over
 6 100 kBq/m². The lower panels show the accumulated dry and wet deposition of ^{137}Cs , the
 7 pattern of dry deposition is quite different from that of ^{131}I and most of the areas have values
 8 lower than 5 kBq/m².



1
 2 Fig. 11. Daily total depositions in station IBARAKI and TOCHIGI with different dry and wet
 3 parameterizations.



1
 2 Fig. 12. Daily total depositions in station GUNMA and TOKYO with different emission rates,
 3 gas partitioning of ^{131}I and size distribution of ^{137}Cs .



1
 2 Fig. 13. Distribution of accumulated total depositions of ^{131}I and ^{137}Cs over domain 2 with
 3 different emission rates. Emission rates estimated by JAEA are used in case REF and those
 4 from TEPCO are used in case EM2.